

AD-A087 142

PRINCETON UNIV N J DEPT OF CHEMICAL ENGINEERING

F/G 11/9

A REVIEW OF APPROACHES TO THE STUDY OF CAVITATION INHIBITION BY--ETC(U)

JUL 80 W R SCHOWALTER, S K HARA

N00014-79-C-0385

UNCLASSIFIED

160-6076-1

NL

142  
AD-A  
797142



END  
DATE  
FILMED  
9-80  
DTIC

Report No. 160-6076-1

LEVEL

11

A REVIEW OF APPROACHES TO THE STUDY OF CAVITATION INHIBITION BY MEANS  
OF POLYMER ADDITIVES

ADA087142

William R. Schowalter and Stuart K. Hara  
Department of Chemical Engineering  
Princeton University  
Princeton, NJ 08544

14 July 1980

Technical Report for Period 15 April - 31 October 1979

Approved for public release; distribution unlimited.

Prepared for  
OFFICE OF NAVAL RESEARCH (CODE 438)  
800 N. Quincy Street  
Arlington, VA 22217

Under Contract N00014-79-C-0385  
Task Number NR 062-637

DTIC  
ELECTED  
JUL 25 1980  
C

Reproduction in whole or in part is permitted for any purpose of the  
United States Government

DDC FILE COPY

80 7 21 06

REPORT DOCUMENTATION PAGE		READ INSTRUCTIONS BEFORE COMPLETING FORM	
1. REPORT NUMBER (14) 160-6076-1	2. GOVT ACCESSION NO. AD-A087142	3. RECIPIENT'S CATALOG NUMBER (9)	
4. TITLE (and Subtitle) A Review of Approaches to the Study of Cavitation Inhibition by means of Polymer Additives		5. TYPE OF REPORT & PERIOD COVERED Technical Report 15 Apr - Nov 1979	
7. AUTHOR(s) (10) William R. Schowalter and Stuart K. Hara		8. CONTRACT OR GRANT NUMBER(s) (15) N00014-79-C-0385 free	
9. PERFORMING ORGANIZATION NAME AND ADDRESS Department of Chemical Engineering Princeton University Princeton, NJ 08544		10. PROGRAM ELEMENT, PROJECT, TASK AREA & WORK UNIT NUMBERS NR 062-637	
11. CONTROLLING OFFICE NAME AND ADDRESS Office of Naval Research (Code 438) 800 N. Quincy Street Arlington, VA 22217		12. REPORT DATE 14 July 1980	
14. MONITORING AGENCY NAME & ADDRESS (if different from Controlling Office) (12) 69		13. NUMBER OF PAGES 61	
		15. SECURITY CLASS. (of this report) Unclassified	
		15a. DECLASSIFICATION/DOWNGRADING SCHEDULE	
16. DISTRIBUTION STATEMENT (of this Report) Approved for public release; distribution unlimited			
17. DISTRIBUTION STATEMENT (of the abstract entered in Block 20, if different from Report)			
18. SUPPLEMENTARY NOTES A review and plan for Mr. Hara's dissertation			
19. KEY WORDS (Continue on reverse side if necessary and identify by block number) cavitation bubbles rheology viscoelastic liquids non-Newtonian fluid mechanics polymers			
20. ABSTRACT (Continue on reverse side if necessary and identify by block number) A review of topics relevant to Newtonian and non-Newtonian bubble and droplet dynamics, together with an extensive bibliography, are presented. This review forms the basis for an assessment of theoretical and experimental studies of nonspherical bubble growth and collapse in non-Newtonian fluids. In the report, which is adapted from a proposition for a research dissertation, we show the difference between extremes of inertia-dominated and viscosity-dominated bubble dynamics under conditions of interest.			

20. ABSTRACT (continued)

→ Comparison with published data shows that the effect of inertia is expected to be important, even in non-Newtonian systems. Finally, the goals of the research are delineated, and possible theoretical and experimental approaches are outlined. ↗

### SUMMARY

An important requirement of all Ph.D. candidates is preparation and defense of what is known as the "first proposition." The proposition is intended to be a review of the literature relevant to the subject of the dissertation, and an outline of the goals and methodology of the dissertation. In the present case Mr. Stuart Hara submitted such a proposition last fall. Because it contains a unique review and assessment of the literature dealing with bubble growth and collapse, we have slightly modified his proposition and have prepared from it the first Technical Report for this contract. The report is of a review nature. However, in Section IV we have carried out some computations to show regions of agreement and disagreement between published theory and experiment. Section V is a description of proposed theoretical and experimental research, some of which is currently underway.

Accession For		<input checked="checked" type="checkbox"/>
NTIS - GAO&I		<input type="checkbox"/>
DAS TAB		<input type="checkbox"/>
Unannounced		
Justification		
By _____		
Distribution/		
Availability Codes		
Dist	Avail and/or	special
A		

## TABLE OF CONTENTS

### Summary

I	Introduction.....	1
II	Newtonian Bubble Dynamics and Drop Deformation.....	4
III	Non-Newtonian Effects.....	17
IV	Preliminary Analyses.....	37
V	Ultimate Plans and Goals for this Research.....	49
VI	Bibliography.....	56

## I INTRODUCTION

Cavitation - the formation and subsequent behavior of gaseous volumes, usually in a continuous liquid phase - has long occupied a prominent position in engineering theory and practice. The damage resulting from aquatic cavitation may be the premier example of the practical importance of this phenomenon. As a result, the study of naval architectural hydrodynamics in particular remains a very active field in which the limited reproducibility and questionable direct applicability of laboratory work continues to challenge workers.

In reviews by Plesset and Prosperetti [65] and Acosta and Parkin [1] a natural concentration on aqueous systems is apparent. Yet, even for this specific Newtonian fluid, the role of geometry, both macroscopic and microscopic, and numerous other possible design variables, remains unclear. Also, two competing regimes which divide the field exist: nucleation or microscopic inception, and bubble or cavity dynamics. The relative importance of each regime varies according to the specific circumstances.

The phenomenon is further complicated by the introduction of dilute macromolecular solutions into experimental systems. Cavitation inception in flow past blunt bodies is definitely inhibited. To measure the state of liquid flow at which cavitation appears, an "incipient cavitation number,"  $\sigma_i$ , has been defined

$$\sigma_i = \frac{P_s - P_v}{1/2 \rho V_o^2} \quad (1)$$

where  $P_s$  is the local free stream static pressure,  $P_v$  the liquid vapor pressure,  $\rho$  is the liquid density, and  $V_o$  the free stream velocity. Ellis, et al. [25, 27] have experimentally found a reduction of  $\sigma_i$  by as much as 70% from its value for tap water for a solution of 300 ppm Guar gum.

That this cavitation inhibition is not merely a nucleation effect is demonstrated by the change in appearance of the cavities upon formation. Ting [83] shows photographs which display cavities which are smaller than their counterparts in

pure water. Hoyt [43] and Ellis, et al. [26] have also commented on this qualitative change in the nature of the cavities.

Ellis and Ting [26, 84] speculated that this cavitation suppression is a manifestation of the elastic properties of a non-Newtonian solution which might similarly inhibit the growth of an individual cavitation bubble. To test this hypothesis, they investigated the spherically symmetric growth of a single bubble in an otherwise quiescent dilute polymer solution [81, 82, 84]. Agreement between theoretical analyses and experiments was good, but in both the presence of the macromolecules retards bubble growth only slightly. Since this retardation is insufficient to account for the cavitation inhibition in flows, another approach must be taken.

Dilute polymer solutions can have strong, and often unexpected, effects on the velocity field of a flow. Acoustic streaming is a prime example [15]. In this case the direction of the secondary flow generated by an oscillating rod is actually reversed by the addition of a small amount of polymer. Theoretical analysis has shown that this reversal is consistent with the stresses introduced by the viscoelasticity of the liquid. Thus, there is a strong possibility that the alteration of overall flow field reduces cavitation effects by changing the stress field around the point of cavitation, both before and after nucleation. A successful analysis of cavitation inhibition is, therefore, expected to require inclusion of the overall flow along with non-Newtonian elastic effects.

The model system proposed here is a single cavitation bubble growing in a specified undisturbed flow of a non-Newtonian fluid. Any analysis of this system involves a coupling between fluid and flow which necessitates the synthesis of manifold disciplines. One is Newtonian bubble dynamics, which has, historically, dealt most completely with spherically symmetric flows. Here, it is necessary to understand the relative importance of the numerous physical effects and parameters which arise. In addition, the imposed flow will often invalidate any assumption of spherical symmetry so the extensive work on small drop deformation, slender

body theory and singularity analysis may be applicable. To include non-Newtonian effects the various constitutive formulations and formalizations should be evaluated. Previous applications of these constitutive relations, particularly to bubbles, are especially important.

In subsequent sections, each of these subjects will be treated in some depth. In addition, several preliminary results attempting to evaluate the importance of various physical effects and to extend some other results will be presented. Further steps of a similar nature are also proposed. Finally, the more ambitious plans for this research are presented. These include some rudimentary ideas for experimental work which will, it is hoped, give guidance for theoretical work and, ultimately, confirm any analytical results.

## II NEWTONIAN BUBBLE DYNAMICS and DROP DEFORMATION

Just as most subsequent researchers have been motivated to study bubbles by interest in cavitation damage, Rayleigh [72, 50] found this field sufficiently appealing to perform the first analysis of bubble dynamics. He solved the problem of the collapse of an empty cavity in a large mass of liquid. Neglecting surface tension, fluid viscosity, and any thermal effects, and assuming spherical symmetry, his result can easily be derived from the equations of motion as

$$\ddot{R}R + \frac{3}{2}\dot{R}^2 = \frac{p(R) - p_{\infty}}{\rho} \quad (2)$$

where  $\rho$  is liquid density,  $p_{\infty}$  is the pressure in the liquid far from the bubble, and  $p(R)$  is the pressure at the bubble boundary, which is also assumed to be the pressure throughout the bubble. The specification of an incompressible fluid implies that the velocity within the liquid is given by

$$u(r,t) = \frac{R^2}{r^2} \dot{R} \quad (3)$$

The neglected surface tension and viscosity terms can easily be included to give a "generalized Rayleigh equation" [65]

$$\ddot{R}R + \frac{3}{2}\dot{R}^2 = \frac{1}{\rho} \left[ p_i - p_{\infty} - \frac{2\sigma}{R} - \frac{4\mu}{R} \dot{R} \right] \quad (4)$$

where  $p_i$  is now the pressure inside the bubble which is assumed to be homogeneous, and  $\sigma$  and  $\mu$  are the surface-tension constant and liquid viscosity, respectively. In the general situation, both  $p_{\infty}$  and  $p_i$  may be functions of time (or of  $R$ ) and  $\sigma$  and  $\mu$  may not be constant. It is also important to emphasize that spherical symmetry is assumed to persist throughout the process.

For pure water,  $\sigma$  and  $\mu$  are weak functions of other physical parameters, such as temperature. This has allowed successful modelling under the assumption of constant values for those two coefficients. However, the composition and behavior of  $p_i$  with the evolution of the bubble is not so simple. Plesset [65] has delineated two categories of bubble dynamics which he has labelled gas bubbles and vapor bubbles. Gas bubbles are those cavities for which the medium in the interior is largely or

completely a permanent, noncondensable gas. For vapor bubbles the gaseous phase consists almost entirely of the vapor of the surrounding fluid.

Gas bubbles have been extensively investigated, particularly in the areas of surface oscillations and mass diffusion effects [see review 65]. They have technological applications to such processes as plastics foaming, but, for the field of cavitation, these gas bubbles are much less relevant than vapor bubbles.

The category of vapor bubbles is subdivided into two other topics. The subclassification is based upon the extent to which thermal effects alter  $p_i$  and thus, bubble behavior. The strong temperature dependences of  $p_i$  equilibrium vapor pressure and vapor density act to significantly reduce  $p_i$  for a growing bubble as evaporation at the bubble surface cools the interior. Using an energy balance, and assuming that heat is supplied by a liquid layer which has thickness comparable to the diffusion length  $(Dt)^{1/2}$ , the "thin thermal boundary layer" assumption, this temperature difference can be estimated as

$$\Delta T \approx \frac{1}{3} \frac{R \rho_v^e(T) L}{(Dt)^{1/2} \rho c_s} \quad (5)$$

where  $L$  is the latent heat of evaporation,  $\rho_v^e(T)$  is the equilibrium vapor density at temperature  $T$ ,  $D$  is the thermal diffusivity, and  $t$  is the time required to grow to radius  $R$ . For water at  $15^\circ\text{C}$ , with  $R=0.1$  cm, and  $t=10^{-3}$  sec,  $\Delta T=0.2^\circ\text{C}$ , while at  $100^\circ\text{C}$ ,  $\Delta T=13^\circ\text{C}$ . For the former case, in which the thermal effect is not expected to be important, the proper term is "cavitation" bubble. In the latter, and all cases where thermal effects dominate inertial effects, the result is "boiling" or "vapor" bubbles.

The cavitation bubble is the simpler case since, with complete neglect of thermal effects,  $p_i = p_v = \text{constant}$ . Then, for a constant  $p_i$  and neglecting viscous effects

$$\dot{R}^2 = \left(\frac{R_0}{R}\right)^3 \dot{R}_0^2 + \frac{2}{3} \frac{p_v - p_\infty}{\rho} \left[1 - \left(\frac{R_0}{R}\right)^3\right] - \frac{2\sigma}{\rho R} \left[1 - \left(\frac{R_0}{R}\right)^2\right] \quad (6)$$

where initial values are signified by the subscript zero. For  $\dot{R}=0$  and again neglecting surface tension, the Rayleigh result

for time to complete collapse is

$$t_o = \frac{r(5/6)}{r(1/3)} \left[ \frac{3\pi \rho}{2(p_\infty - p_v)} \right]^{1/2} R_o \doteq 0.915 \left( \frac{\rho}{p_\infty - p_v} \right)^{1/2} R_o \quad (7)$$

Quantitative experimental confirmation of this value was given by Lauterborn [52]. He was able to generate "empty" cavities by focusing a pulse from a Q-switched ruby laser on a point on the interior of a liquid mass. Agreement between experiment and equation (7) was excellent, despite the actual compressibility of the liquid. Note that this compressibility is expected to become significant in the final stages of collapse, when the Mach number of the bubble wall becomes large.

To analyze the more complicated vapor bubbles, it is necessary to solve the energy equation along with the coupled Rayleigh equation. Plesset and Zwick [66, 67] found that under the assumption of a thin thermal boundary layer, the temperature at the bubble wall is approximately

$$T = T_\infty - \left( \frac{D}{\pi} \right)^{1/2} \frac{L\rho'}{k} \int_{x=0}^t \frac{R^2(x) \dot{R}(x)}{[\int_x^t R^4(y) dy]^{1/2}} dx \quad (8)$$

where  $T_\infty$  is the temperature at infinity,  $D$  is the liquid thermal diffusivity,  $L$  is the latent heat of evaporation,  $\rho'$  is vapor density, and  $k$  is the thermal conductivity of the liquid. The growth of the vapor bubble is governed by numerous parameters, including  $A$  which gives a linear approximation to the relationship between vapor pressure  $p_v(T)$  and  $T$

$$\frac{p_v(T) - p_o}{\rho} = A (T - T_b) \quad (9)$$

where  $T_b$  is the boiling temperature at pressure  $p_o$ . Other constants are defined as

$$\alpha = \left( \frac{2\sigma}{\rho R_o} \right)^{1/2} \quad (10A)$$

$$\mu = \frac{AL\rho'}{3kR_o\alpha} \left( \frac{D}{\pi\alpha} \right)^{1/2} \quad (10B)$$

and  $\beta$ , which is implicitly given as a root of

$$\beta^2 + 3\mu(\pi\beta)^{1/2} - 1 = 0 \quad (10C)$$

If the mechanism by which growth is triggered from an initial equilibrium radius  $R_o$  is a constant heat source per unit volume

of strength  $a$ , such that

$$\eta = at \quad (10D)$$

then the bubble evolution can be divided into four regimes [93]. The two most easily understood are the first, a "delay" period, and the fourth, where growth approaches an asymptotic limit.

The initial growth occurs when radial increase is so rapid that the change in bulk temperature, which follows from equation (10D), is insignificant. To first order, the solutions to the governing equations are

$$\dot{R} = R_0 \left[ 1 + \frac{2\gamma}{\beta(3\beta^2+1)} \exp(\alpha\beta t) \right] \quad (11A)$$

$$T(R) = T_0 - \frac{R_0^2 \alpha^2}{A} \frac{2\gamma(1-\beta)}{\beta(3\beta^2+1)} \exp(\alpha\beta t) \quad (11B)$$

where

$$\gamma = (ADa)/(\alpha R_0^3 k) \quad (12)$$

The delay period is very short, but results in a new value of  $R$ , slightly larger than  $R_0$ , from which "important" growth begins.

When  $R \gg R_0$ , the heat diffusion has a limiting effect on  $\dot{R}$ . A consistent solution to the equations of motion and energy which takes into account the delay period is generated using an asymptotic expansion. The leading terms of this solution are

$$R \approx R_0 \left( \frac{2}{\pi\mu} \right) \left( \frac{\alpha t}{3} \right)^{1/2} \left[ 1 + O(t^{-1/2}) \right] \quad (13A)$$

$$T = T_0 - \frac{\alpha^2 R_0^2}{A} \left[ 1 + O(t^{-1/2}) \right] \quad (13B)$$

The two intervening regimes can be thought of as intermediate behaviors necessary for patching together the first and last time periods. Notice that  $\dot{R} \propto t^{-1/2}$  is a decreasing function of time in the asymptotic regime.

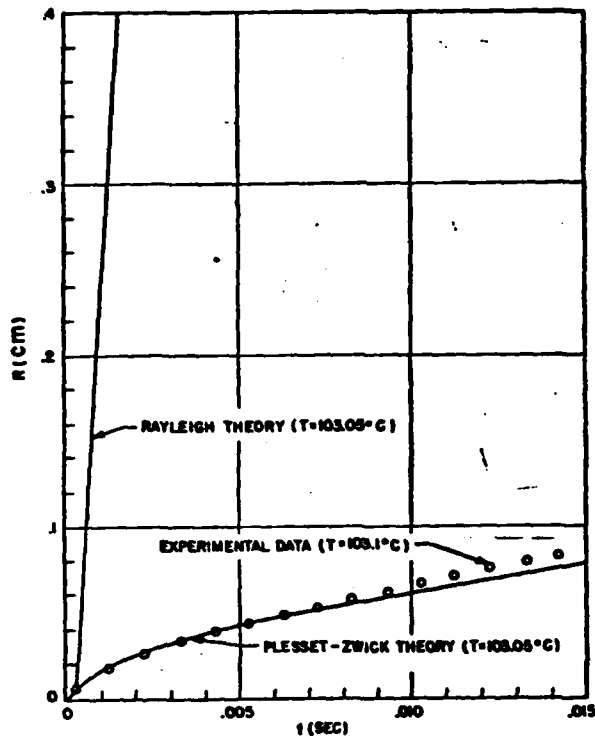


FIG. 1 [23]

The large magnitude of the thermal effect on boiling bubbles is illustrated in figure 1. Here the theoretically predicted radius vs. time profiles for the Plesset analysis is shown along with the Rayleigh result for water at  $103^{\circ}\text{C}$ . Excellent experimental agreement with the Plesset prediction was found by Dergarebedian [23]. He used a Q-switched ruby laser to generate bubbles under conditions closely approximating the theoretical situation.

Zwick and Plesset [93] have also analyzed the collapse of a bubble including the heating effect caused by condensation of the vapor.

Here numerical techniques are definitely required since the expected large temperature differences do not allow simple analytic expressions for vapor pressure or vapor density. Evidently, the time scale for collapse is so small that the dynamics of the process vary only slightly from the Rayleigh solution (See figure 2).

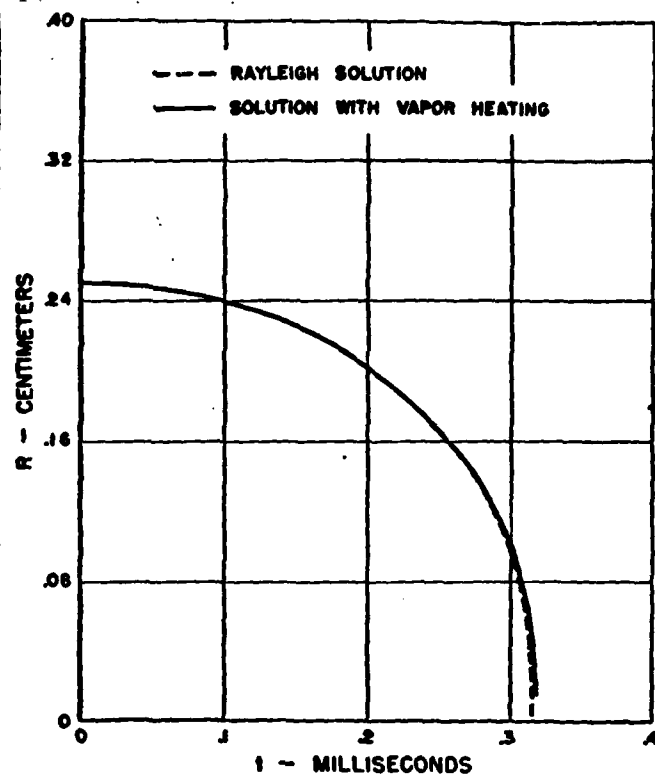


FIGURE 2 [93, P.3238]

These analyses all contain the premise of a spherically symmetric bubble. Plesset [61] initially performed a linear stability analysis on the nearly spherical interface between two immiscible, incompressible, inviscid fluids. He assumed an initial drop shape given by

$$r_s = R + a(t) Y_n \quad (14)$$

where  $Y_n$  is a spherical harmonic of degree  $n$  [50, 54, 88, 92] and  $a$  is initially small. The analysis proceeded conventionally in order to determine the conditions for which  $a(t)$  will grow, implying the shape is unstable, and those for which it will not, implying stability. One finds that

$$a(t) = \alpha(t) \left( \frac{R_0}{R} \right)^{3/2} \quad (15)$$

$$\text{with} \quad \ddot{\alpha} - G(t) \alpha = 0 \quad (16A)$$

$$G(t) = \frac{3}{4} \frac{\dot{R}^2}{R^2} + \frac{\ddot{R}}{R} \left[ \frac{3}{2} + \frac{n(n-1)\rho_2 - (n+1)(n+2)\rho_1}{n\rho_2 + (n+1)\rho_1} \right] \quad (16B)$$

$$- \frac{(n-1)n(n+1)(n+2)\sigma/R^2}{R[n\rho_1 + (n+1)\rho_2]}$$

where  $\sigma$  is the surface tension constant and  $\rho_1$  and  $\rho_2$  are the fluid densities of the interior and exterior liquids, respectively. Thus

$$\begin{aligned} G(t) < 0 & \quad \text{promotes stability} \\ G(t) > 0 & \quad \text{promotes instability.} \end{aligned} \tag{17}$$

This means that surface tension always has a stabilizing effect, and from (15), increasing  $R$  or bubble growth is seen to have a stabilizing effect, while the opposite, bubble collapse, promotes instability.

Plesset and Mitchell [64] then performed a more involved analysis for a vapor cavity, neglecting the density of the vapor and the viscosity of the vapor and the liquid. Results showed that, for an expanding vapor cavity, if  $|a(0)|/R \ll 1$ , then  $|a(t)|/R(t) \ll 1$ . For a collapsing cavity distortion amplitudes remained small so long as  $1.0 \geq R/R_0 \geq 0.2$ , but as  $R \rightarrow 0$ ,  $a(t)$  increased as  $R^{-1/4}$ . Thus the spherical shape is unstable for the later stages of bubble collapse. These trends are valid even when a small viscous effect is included in the treatment [70]. Viscosity does tend to damp the growth in amplitude of the higher order harmonics.

To determine bubble shape stability, no characteristics of the deformation beyond its existence and magnitude were necessary, a direct result of the far-field conditions. The bubbles were assumed to exist in an infinite fluid, quiescent apart from the direct effects of the cavity; this is a spherically symmetric geometry giving an equilibrium shape with similar character. Of course, this is not the only circumstance in which a bubble may arise. There may be conditions imposed on the fluid away from the bubble, such as an elongational flow or a solid boundary, or the bubble may be initialized as nonspherical and a detailed description of its evolution desired. Bubbles have provoked some study in this regard, but more often liquid drops and solid bodies have been examined, giving rise to general techniques for nonspherical shapes.

For bubbles and all initially spherical bodies in an imposed flow, the primary method of study has been expansion of the velocity profile in terms of spherical harmonics [76]. Use of this method is predicated upon an assumption of creeping flow, at least in the immediate vicinity of the bubble. Under this restriction, Happel and Brenner [38, sect 3-2] offer a practical presentation of the use of spherical harmonics, Lamb's General Solution [50]. The pressure field must satisfy

$$\nabla^2 p = 0 \quad (18)$$

This suggests expanding  $p$  as a series of solid spherical harmonics  $p_n$ .

$$p = \sum_{n=-\infty}^{\infty} p_n \quad (19)$$

Then Lamb's General Solution for velocity  $\underline{v}$  is

$$\underline{v} = \sum_{n=-\infty}^{\infty} \left[ \nabla \chi(\underline{r} X_n) + \nabla \phi_n + \frac{(n+3)}{2\mu(n+1)(2n+3)} \nabla^2 p_n - \frac{n}{\mu(n+1)(2n+3)} \underline{r} p_n \right] \quad (20)$$

where  $\chi$  and  $\phi$  are each solid spherical harmonics given as the series of solutions to

$$\nabla^2 \chi = 0 \quad (21A)$$

$$\nabla \cdot \underline{v} = 0 \quad (21B)$$

Happel and Brenner proceed to describe the determination of the  $p_n$ ,  $\chi_n$  and  $\phi_n$  for given boundary conditions.

Einstein [24] was able to calculate an equivalent viscosity  $\eta^*$  for a dilute suspension of rigid spheres without using spherical harmonics. His result

$$\eta^* = \eta \left( 1 + \frac{5}{2} a^3 \right) \quad (22A)$$

$$a^3 \ll 1 \quad (22B)$$

where  $\eta$  is the viscosity of the dispersing fluid and  $a^3$  is the volume fraction of spheres, was rederived using a harmonic expansion by Fröhlich and Sack [32]. They were also able to calculate the viscous and elastic properties of a substance equivalent to a dilute suspension of elastic spheres in a steady elongational flow. The non-rigidity of these elastic spheres introduces the need to calculate the deformation which would result if these same stresses were present for the elastic

spheres. In assuming this to give an accurate description of the non-sphericity, the deformation is required to be small and not to perturb the flow significantly. In considering the behavior of a viscous drop in the flow of a viscous, Newtonian fluid, two important parameters are found to be

$$\lambda = \mu^*/\mu_o \quad (23A)$$

$$k = \sigma/\mu_o Ga \quad (23B)$$

where  $\mu^*$  is the the viscosity inside the drop,  $\mu$ , that of the surrounding fluid,  $\sigma$  the surface-tension constant,  $a$  is the radius of the drop and  $G$  some measure of flow strength. Taylor [78] discussed the result for a simple shear flow, and found two limiting cases. For the first, with  $\lambda=O(1)$  and  $k \gg 1$ , termed the interfacial tension dominated case, the drop deforms, to order  $(1/k)$ , into a spheroid with its major axis  $45^\circ$  to the flow. For the second, with  $k=O(1)$  and  $\lambda \gg 1$ , to  $O(1/\lambda)$ , the major axis is aligned with the flow. Taylor and Acrivos [79] found that a falling drop was deformed into an oblate spheroid when surface tension dominates, and has spherical caps as surface tension becomes less important. They also performed higher order calculations by re-evaluating the flow around the deformed drop.

A general time dependent flow containing a viscous drop, and other, more specific, flow situations have been analyzed by Cox [20], Frankel and Acrivos [31], Barthes-Biesel and Acrivos [4], and others [36, 37]. The viscosity ratio  $\lambda$  (23a) and ratio of surface tension to flow strength  $k$  (23b) remain important parameters. In the notation of Cox [20], the deformed surface is given by

$$r = 1 + \epsilon f(r_i/r) \quad (24)$$

where  $\epsilon$  is a small parameter. The function  $f$  is expanded in terms of spherical surface harmonics as

$$f = \sum_{pq} P_{pq} \left[ \frac{\partial^2}{\partial r_p \partial r_q} (1/r) \right]_{r=1} \quad (25)$$

Bakimi [36] presents experimental results which compare well with theoretically derived values for  $P_{pq}$ . His work made use of an

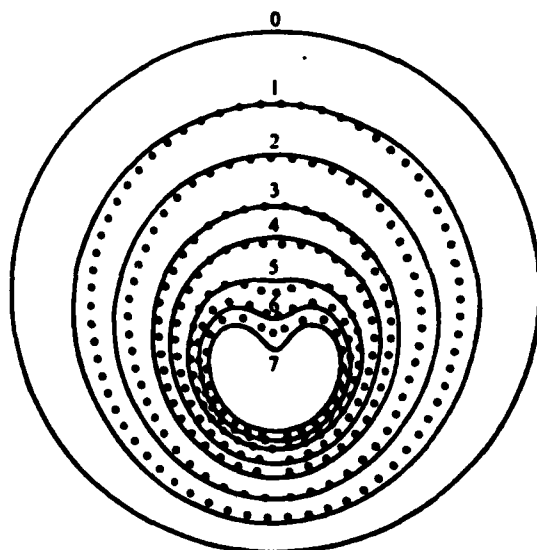
orthogonal rheometer to generate flow fields with variable contributions from vorticity and deformation. Despite this success, there is "some confusion" among various workers about the equations to be solved in determining the  $P$ . Ballison [71] attempts to unify these differing results, and in so doing concludes that, within the range of validity of this analysis, there are at least three special cases in which an equilibrium shape may be achieved. These special cases are:

Weak flow -  $k \gg 1$  with  $\lambda = o(k)$

High viscosity drops -  $\lambda \gg 1$  with  $k = o(\lambda)$

High viscosity with comparably weak flow -  $k, \lambda \gg 1$

For bubble dynamics, only the first case may be useful.



----- Solid boundary -----

Comparison of experimentally determined bubble shapes (open circles) on collapse of a spherical bubble near a plane solid wall with theoretical curves taken from Plesset & Chapman (1971) (solid curves). The framing rate is 300 000 frames/s, the maximum bubble radius  $R_{max} = 2.6$  mm, the distance of the bubble centre from the wall  $b = 3.9$  mm and  $b/R_{max} = 1.5$ .

Curve	0	1	2	3	4	5	6	7
Time, $R_{max}(\rho_b/\Delta p)^{1/2}$	0	0.725	0.825	0.961	0.991	1.016	1.028	1.036

( $\rho_b$  is the density of the liquid and  $\Delta p$  is the constant difference between the ambient liquid pressure and the pressure in the cavity.)

FIGURE 3 [63, P.396]

The presence of a solid boundary in the vicinity of a bubble alters the flow created by the cavity dynamics. In the collapse process a cumulative jet is formed which may be one of the major causes of the destructive action of cavitation. Experimentally, the jet has been observed in laser-induced bubbles [53], with qualitative agreement achieved with numerical calculations [65] (See figure 3). The theoretical model, however, does not generate jet speeds sufficient for the destruction encountered in practice, so that other factors such as nonspherical initial shape have been investigated [70].

An initial nonsphericity is important even in the absence of an imposed flow or solid boundary.

The requisite mathematics has been put forth by Hsieh [45], who includes equations for heat and mass transfer effects, compressibility and suggests variational methods. Simplified numerical results by other authors [17] show that an initially prolate spheroid (figure 4a) will form two jets upon collapse, while an oblate spheroid (figure 4b) leads to a dumbbell form. These nonlinear results were compared with the linear theory

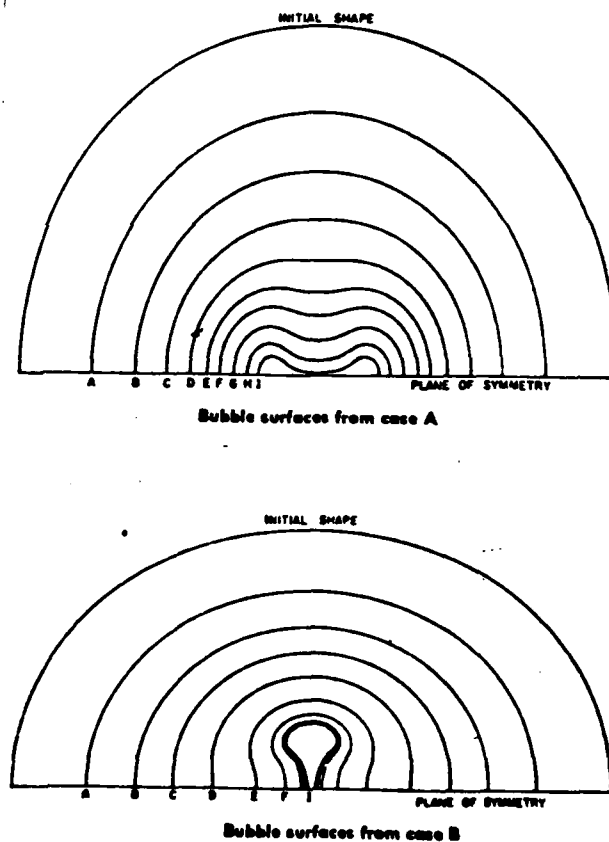


FIGURE 4 [17]

developed

by Plesset and Mitchell [64] in their detailed stability analysis and good agreement was found until the final stages of collapse.

The success of the linear analysis in predicting bubble behavior even for large deformations is a pleasant surprise. However, such analyses, which begin from perfect spheres, cannot be expected to have such a large range of validity. Even the cited linear analysis eventually becomes invalid. Nonetheless, these shapes are important; there is a strong possibility that bubble dynamics will generate highly deformed shapes in certain imposed flows since the small viscosity ratios  $\lambda$  (23a) present do not result in a "small deformation" equilibrium, in the sense of Ballison [71], unless the flow strength is very low, or surface tension dominates. The most common method for dealing with highly deformed bodies is called slender body analysis. The theory neglects inertial effects and, as the name suggests, has been created for flows around long, slender, solid bodies characterized by small thickness ratios  $\kappa$ .

$$\kappa = b/l \ll 1 \quad (26)$$

where the cross-sectional radius is of order  $b$ , and  $l$  is the length of the body.

Slender body theory was initiated by Burgers [13], when he attempted to determine the force on a long, slender ellipsoid of revolution at rest in a uniform translational motion  $U$ . He began the analysis by assuming the disturbance produced by the body was like that which would result from a line of force on the symmetry axis, which is of magnitude

$$\begin{aligned} f(z) &= A_0 + A_2 (z/a)^2 + A_4 (z/a)^4 & |z| < a \\ f(z) &= 0 & |z| \geq a \end{aligned} \quad (27)$$

where  $a$  is the semi-major axis,  $z$  is the distance along the axis from the center of the ellipsoid, and  $A_0$ ,  $A_2$ , and  $A_4$  are constants. He was able to derive

$$f = \frac{4\pi\mu a U}{\ln(2a/b) - 0.5} \quad (28)$$

which is the limiting form of the result obtained for spheroids of finite cross-section. Subsequent efforts in this field by other workers have extended this type of analysis to non-uniform cross-sections [6], shear flows [21(2)], and even curved axes [21(1)]. In all cases, the intended result is the function  $F(z)$  which best matches boundary conditions, and is often obtained using matched inner and outer expansions. From  $F(z)$ , the forces and torques on the body can be calculated.

A single function  $F(z)$  can give exact results only in the limit as  $\kappa \rightarrow 0$ . This function  $F(z)$  can equivalently be considered the distribution along the axis of point singularities in the flow field, or Stokeslets [5]. The velocity and pressure field due to a Stokeslet  $F_j$  [11] is

$$u_i = \frac{F_j}{8\pi\mu} \left[ \frac{\delta_{ij}}{r} + \frac{r_i r_j}{r^3} \right] \quad (29A)$$

$$p = \frac{F_j}{4\pi} \frac{r_j}{r} \quad (29B)$$

For bodies of finite cross-section, it is only possible to generate exact solutions to Stokes flow problems by determining the proper spatial distribution of Stokeslets and the other fundamental singularities (figure 5), which can be derived from the derivatives of the Stokeslet [11]. Thus, just as small deformation methods may be valid for finite deformations, the slender body singularity technique is extendable to finite thickness ratios. Most shapes are analyzable, at least for Stokes flow and rigid bodies.

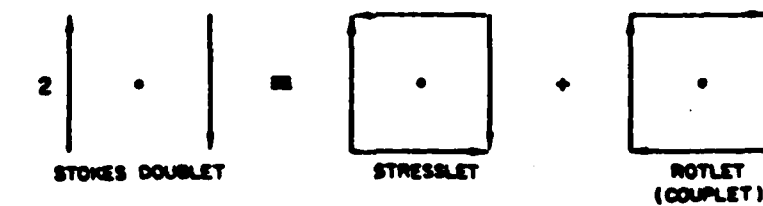


FIGURE 5 [11, P.25]

### III NON-NEWTONIAN EFFECTS

Many instances of seemingly anomalous behavior of non-Newtonian fluids are well-documented. Two of the most commonly cited examples are rod climbing or the Weissenberg effect [8, P.92], and extrudate or "die" swell [8, P.102]. Schowalter [74] emphasizes the "counter-intuitive" nature of these effects, and explains that this is a consequence of the Newtonian character of that very common fluid, water, which is the basis for such intuition. While water, and all truly Newtonian fluids, exhibit no elastic forces, non-Newtonian fluids often do, and the existence of such forces can be used to explain many of the unexpected effects.

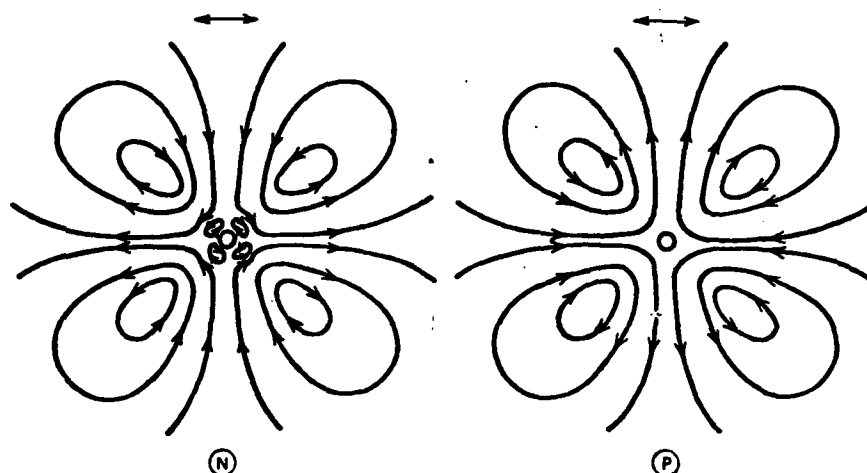
Several of these effects can be viewed as exhibitions of fluid properties which are also relevant to cavitation inhibition, particularly those properties which involve a free surface or result in a macroscopic alteration of the flow and/or pressure field. In the first category, examples include:

- jet stability - in a Newtonian fluid, breakup of a free jet occurs in clearly defined waves. Such definition is not apparent for fluids which exhibit elastic properties [74, P.3].

- open channel flow - for many non-Newtonian fluids, the free surface of the liquid when flowing down an open, inclined channel is convex, it is virtually flat for the Newtonian case [8, P.105].

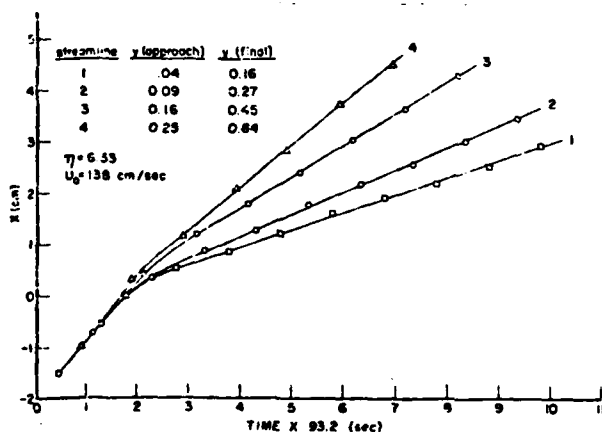
Demonstrations of the second type of effect are necessarily more involved, requiring some flow visualization or measurement techniques. Yet there are good examples, including:

- secondary flow induced by an oscillating cylinder - as previously cited, Chang [15] observed reversal of secondary flow (figure 6) for polyacrylamide solutions as dilute as 20-30 ppm. He also found the situation amenable to analysis.

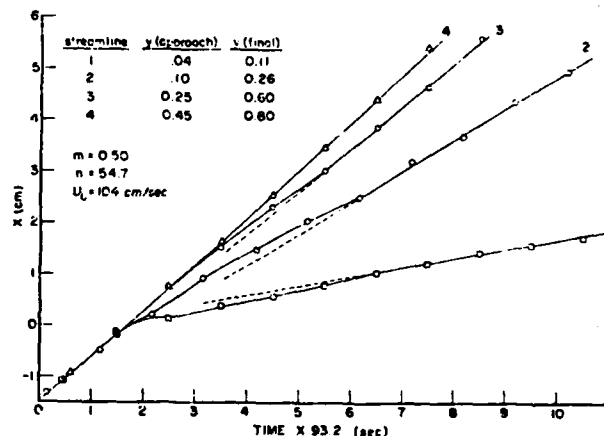


Secondary flow produced by a long cylinder oscillating normal to its axis. The cylinder is viewed on end and the direction of oscillation is shown by the double arrow. (N) A water/glycerin mixture moves away from the cylinder along the axis of oscillation. (P) The direction of the secondary flow is reversed when 100 ppm polyacrylamide (Separan AP 30) is added to the water/glycerin mixture.

FIGURE 6 [16]



Particle position vs. time for Newtonian fluid (fluid 4).



Particle positions vs. time for viscoelastic fluid (fluid 3).

FIGURE 7 [41, p. 257]

flow past a flat plate - experimental results [41] show definite changes in particle position (figure 7) and fluid velocity (figure 8) when a Newtonian liquid is replaced by a viscoelastic fluid in a flow with this simple geometry.

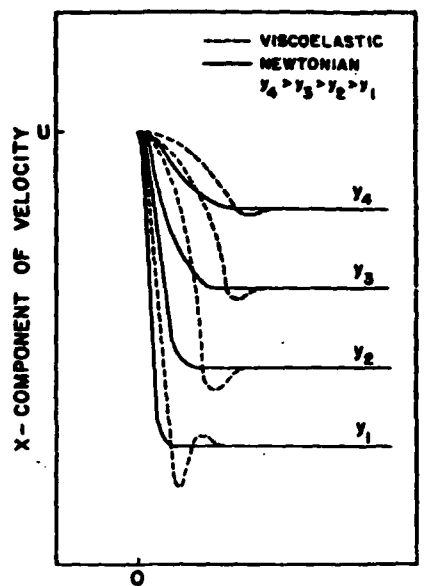


FIGURE 8 [41, P.257]

Finally, a most puzzling instance of non-Newtonian behavior, and one which actually involves bubbles, arises in the recent experimental work of Hassager [40]. He photographically demonstrates the existence of a knife-edged, asymmetric "negative wake" behind a bubble rising in a non-Newtonian fluid. There are many unanswered questions here, most of which have relevance to cavitation inhibition.

To theoretically analyze the flow of any material, it is necessary to construct a model, which, if successful, will "accurately" predict the stress field in that material or class of materials under varying conditions of motion. Such a model is called a constitutive equation and is often formulated to determine the stress tensor  $\mathbf{S}$  for given material conditions, present and past. The constitutive equation must satisfy numerous physical principles and ideally will cover a broad range of materials, but this breadth should not impair its practical applicability.

For non-Newtonian fluids, any attempt to formulate a generally applicable constitutive equation is complicated, and often stymied, by the negative nature of the definition of this

class of matter -

**Non-Newtonian Fluid:** All fluids which are not Newtonian.  
Under the constraint of incompressibility,

$$\nabla \cdot \underline{v} = 0 \quad (30)$$

where  $\underline{v}$  is the vector velocity in the fluid. The constitutive equation for a Newtonian fluid is

$$\underline{S} = -p\underline{I} + \underline{T} \quad (31A)$$

$$= -p\underline{I} + \mu [\nabla \underline{v} + (\nabla \underline{v})^T] \quad (31B)$$

where  $p = -(1/3) \text{tr } \underline{S}$ ,  $\underline{T}$  is the extra stress tensor, and  $\mu$  is the Newtonian fluid viscosity. For a sufficiently simple flow, the essential feature of this relation can be rewritten as

$$\tau = \mu \dot{\epsilon} \quad (32A)$$

where  $\tau$  is now the extra stress,  $\epsilon$  is strain, and the dot denotes time differentiation. A similar relationship for a purely elastic material is

$$\tau = K\epsilon \quad (32B)$$

where  $K$  is the elastic modulus. The presence of viscous forces and elastic recovery in many non-Newtonian effects suggests the combination of these two constitutive relations to describe non-Newtonian behavior. Connecting elements exhibiting viscous damping and elastic recovery in series, the Maxwell element, figure 9, arises, with its constitutive relation

$$\tau + \lambda \dot{\tau} = \mu \dot{\epsilon} \quad (33)$$

Other simple combinations of the elastic and viscous elements result in other linear viscoelastic equations, including

$$\tau + \lambda \dot{\tau} = \mu (\dot{\epsilon} + \lambda' \ddot{\epsilon}) \quad (34)$$

Further sophistication is possible by including multiple values of viscosity and modulus; the adjustment of these values allows better agreement with certain experimental data.



FIGURE 9 Maxwell Element

The two equations (33) and (34) are differential representations. The Maxwell element can also be described in

integral form as

$$\tau(t) = 2(\mu/\lambda) \int_0^t \exp[-(t-t')/\lambda] e(t') dt' \quad (35)$$

This integral form introduces the notion of a memory function. The exponential kernel of the integrand weights the contributions to  $\tau(t)$  by the strain  $e(t')$  at past times  $t'$ . By its mathematical properties, this exponential memory function places more emphasis on recent values of  $e$ . This distribution satisfies a common-sense concept formally stated as the principle of fading memory.

These linear viscoelastic models, which employ simple time differentiation, cannot be generally valid because they do not satisfy another prescription for constitutive equations, the principle of material objectivity. The mathematical criteria for satisfaction of this principle are complex, but the concept is simple; the behavior of a material as calculated for a given model must be independent of observer or frame of reference. The lack of "frame-indifference" of equation (33) means that the calculated response of a material which obeys this equation, when placed on a rotating table, would vary with the rate of this rotation, even when inertial and relativistic effects are neglected.

Another way to view this difficulty with an equation like that for the Maxwell model is to recognize the ambiguous nature of any measure of relative strain for non-infinitesimal deformation. To illustrate, consider a bar of length  $l$  which is stretched to length  $l+\Delta l$ , figure 10.

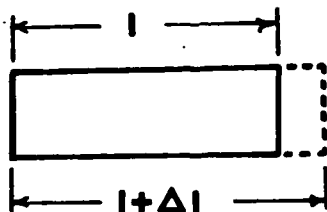


FIGURE 10  
STRAIN

In the limit of infinitesimal strain, as  $\Delta l \rightarrow 0$ , the relative strain is given by two equivalent expressions

$$\lim_{\Delta l \rightarrow 0} \frac{\Delta l}{l} = \lim_{\Delta l \rightarrow 0} \frac{\Delta l}{l + \Delta l} \quad (36)$$

However, if  $\Delta l$  increases, these two expressions are no longer equivalent, and there is no natural choice between them which is generally valid. To use such measures without discrimination implicitly restricts their validity in flow to infinitesimal relative strain.

The restriction to infinitesimal relative strain is a first example of the specificity of certain models to limited types of flow. The intimacy of the relationship between flow and material behavior is illustrated very well by the simplification of  $\underline{S}$  which obtains when the tensor is evaluated for a common class of flows, steady laminar shear flows. Steady laminar shear flows are characterized by a geometry which grants a natural orthogonal coordinate system. The flow is restricted to having a velocity in only one coordinate direction, labelled 1, which varies with respect to only one other direction, 2. If the extra stress  $\underline{T}$  is defined for an incompressible non-Newtonian fluid as it was for the Newtonian case, (31A)

$$\underline{T}(t) = \underline{S}(t) + p\underline{I} \quad (37A)$$

where 
$$p = -\frac{1}{3} \text{tr } \underline{S} \quad (37B)$$
 Then restrictions on  $\underline{T}$  can be found from components of the general equation of motion

$$\rho \frac{Dv}{Dt} = \rho g - \text{grad } p + \text{div } \underline{T} \quad (38)$$

The result is

$$\underline{T} = \begin{vmatrix} t_{(11)} & t_{(12)} & 0 \\ t_{(21)} & t_{(22)} & 0 \\ 0 & 0 & t_{(33)} \end{vmatrix} \quad (39A)$$

$$\text{tr } \underline{T} = 0 \quad (39B)$$

Also,  $\underline{T}$  can only vary with the shear rate  $\kappa$  and is symmetric. Thus, three material functions,  $\tau$ ,  $N_1$ , the first normal stress difference and  $N_2$ , the second normal stress difference, completely specify the tensor  $\underline{T}$ . In one notation [74], they are given by

$$\tau(\kappa) = t_{(12)} = t_{(21)} \quad (40A)$$

$$N_1(\kappa) = t_{(11)} - t_{(22)} \quad (40B)$$

$$N_2(\kappa) = t_{(22)} - t_{(33)} \quad (40C)$$

$$\kappa^0 dv_1/dx_2 \quad (40D)$$

For a Newtonian fluid, both normal stress differences are zero. It is the non-zero value of these quantities which is manifest in such instances of "counter-intuitive" behavior as the Weissenberg effect. These values can be measured. Commonly employed viscometer flows are analyzable as steady laminar shear flows, and have predictive value.

The characterization of a non-Newtonian fluid afforded by measurement of the three material functions (40), although useful and relatively simple, is not complete; the degeneracy in  $\underline{T}$  and exclusive dependence on shear rate  $\kappa$  is flow-specific. The simple linear viscoelastic models are also useful, but unsatisfactory in a general situation. These complications suggest a "retreat" to more basic properties and to a foundation for a constitutive equation or model. Noll [55, 85, 86] has presented the most elegant treatment. His formulation for the most general constitutive equation for a body is

$$\underline{S}(X, t) = \underline{\mathcal{F}}_{t, X}(X) \quad (41)$$

where  $\underline{\mathcal{F}}_{t, X}(X)$  is a functional of the motion of the body from all past time to the present time  $t$ . By invoking physically reasonable assumptions, and retaining the defining equations (37a) and (37b), Noll postulates the constitutive relation for an incompressible simple fluid

$$\underline{T}(t) = \underline{\mathcal{F}}_{s=0} [\underline{C}_{(t)}(s)] \quad (42)$$

where  $\underline{\mathcal{F}}$  is a functional,  $\underline{C}_{(t)}(s)$  is related to the relative deformation gradient, and  $s$  is a dummy variable used to denote the dependence on all past time. This constitutive equation is simple in form, elegant, and contains only a few restrictions. If more assumptions are made, equation (42) assumes a more specific form. Rivlin and Ericksen [73] restricted the time dependence of  $\underline{T}$  to  $s=0$  (near the present) and performed a series expansion. In their notation

$$\underline{T}(t) = \underline{P}(\underline{A}_1, \underline{A}_2, \dots, \underline{A}_n) \quad (43)$$

where the  $\underline{A}_i$  are the Rivlin-Ericksen tensors, functions of the

velocity gradient  $\underline{L}$ , given by

$$\underline{A}_n = \underline{L}_n + \underline{L}_n^T + \sum_{i=1}^{n-1} \binom{n}{i} \underline{L}_i^T \underline{L}_{(n-i)} \quad (44)$$

A form such as (43), though more restricted than that of (42) is still not very useful, and special cases must be examined. If the dependence on all Rivlin-Ericksen tensors higher than the second is suppressed, and  $\underline{F}$  meets certain mathematical conditions, it can be expanded as

$$\underline{T} = \alpha_0 \underline{A}_1 + \alpha_1 \underline{A}_2 + \alpha_2 \underline{A}_1^2 + \alpha_3 \underline{A}_2^2 + \alpha_4 (\underline{A}_1 \underline{A}_2 + \underline{A}_2 \underline{A}_1) + \dots \quad (45)$$

Despite all of these restrictions, equation (45) is still cumbersome and in practice it is often truncated after two terms. This yields the equation for a "second order fluid," which has been found to be of value in some circumstances.

Another approach to constitutive equations has been motivated by the usefulness of the linear viscoelastic equations and the existence of some physical meaning for the constants. For general situations, it is necessary to modify these equations so that they satisfy material objectivity. Oldroyd [56] recognized that the problem originated in the taking of the time derivative for a coordinate basis which is fixed in the "laboratory" reference frame. He suggested manipulations with respect to coordinates inherent to the body. The result has been the formulation and use of many specialized types of derivatives which are implicitly materially objective. These include the codeformational derivative and the corotational or Jaumann derivative. The Jaumann derivative is given, in tensor index notation, by

$$\frac{D}{Dt} a_{ij} = \frac{\partial}{\partial t} a_{ij} + v^k a_{ij,k} - \omega_i^k a_{kj} - \omega_j^k a_{ik} \quad (46)$$

where  $v$  is the velocity and  $\omega$  vorticity. Many constitutive equations have been formulated using these derivatives [8], including the corotational Jeffreys model

$$\underline{T} + \lambda_1 \frac{D}{Dt} \underline{T} = 2\mu (\underline{D} + \lambda_2 \frac{D}{Dt} \underline{D}) \quad (47)$$

where  $\underline{D}$  is the rate of deformation. From consideration of the

applicable mathematical properties, Oldroyd added nonlinear terms in  $\underline{T}$  and  $\underline{D}$  to give the Oldroyd eight-constant model which, in Cartesian coordinates, is

$$\begin{aligned} (1 + \lambda_1 \frac{D}{Dt}) t_{ij} + \mu_0 t_{kk} d_{ij} - \mu_1 (t_{ik} d_{kj} + t_{kj} d_{ik}) + \nu_1 t_{kl} d_{kl} \delta_{ij} \\ = 2\mu [d_{ij} + \lambda_2 \frac{D}{Dt} d_{ij} - 2\mu_2 d_{ik} d_{kj} + \mu_2 d_{kl} d_{kl} \delta_{ij}] \end{aligned} \quad (48)$$

where  $t_{ij}$  and  $d_{ij}$  are the components of  $\underline{T}$  and  $\underline{D}$ , respectively.

Just as differential forms such as equation (33) suggest integral forms like equation (35), corotational derivatives such as equation (46) can be utilized in materially objective integral equations. Such equations can be generalized, in a manner similar to the generalization of the corotational Jeffreys model to the Oldroyd eight-constant model, to give the Goddard memory-integral expansion

$$\begin{aligned} \underline{T} = - \int_0^t G_I(t-t') \dot{\underline{\Gamma}}' dt' - (1/2) \int_0^t \int_0^t G_{II}(t-t', t-t'') [\dot{\underline{\Gamma}}' \cdot \dot{\underline{\Gamma}}'' + \dot{\underline{\Gamma}}'' \cdot \dot{\underline{\Gamma}}'] dt'' dt' \\ - (1/2) \int_0^t \int_0^t \int_0^t \{ 2G_{III}(t-t', t-t'', t-t''') \dot{\underline{\Gamma}}' \dot{\underline{\Gamma}}'' : \dot{\underline{\Gamma}}''' \\ + G_{IV}(t-t', t-t'', t-t''') [\dot{\underline{\Gamma}}' \cdot \dot{\underline{\Gamma}}'' \cdot \dot{\underline{\Gamma}}''' + \dot{\underline{\Gamma}}'' \cdot \dot{\underline{\Gamma}}'' \cdot \dot{\underline{\Gamma}}'] \} dt''' dt'' dt' - \dots \end{aligned} \quad (49)$$

where  $\underline{\Gamma}''$  is a generalized strain tensor at  $t''$ , and the  $G_I$ ,  $G_{II}$ ,  $G_{III}$ , etc. are an infinite series of kernel functions.

These are only a few of the many constitutive equations which have been formulated. More extensive compilations can be found in sources such as Bird, et al. [8]. Several different models are still necessary because no single formalization has been conclusively demonstrated to be preeminent; the usefulness and applicability of each is often flow-specific and imperfect. Despite these limitations, in a given flow situation it is often possible to characterize a fluid sufficiently so that semi-quantitative agreement and prediction can be made.

Critical evaluation of constitutive equations has been hampered considerably by experimental constraints. The most common experimentally achievable flows are vicometric. These are usually approximations to steady laminar shear flow, with the resultant simplification of the measurable extra stress tensor  $\underline{T}$ ,

see equation (39). The degeneracy in  $\underline{T}$  results in a degeneracy in constitutive models; several predict the same behavior, which leaves no basis for comparison. This has led experimentalists to attempt to generate non-viscometric flows, particularly elongational flows. A uniaxial elongational flow is defined by velocity vector and rate of deformation tensor of the form

$$\underline{V} = [v_1(x_1), -v_1(x_2)/2, -v_1(x_3)/2] \quad (50A)$$

$$\underline{D} = \dot{\epsilon} \begin{vmatrix} 2 & 0 & 0 \\ 0 & -1 & 0 \\ 0 & 0 & -1 \end{vmatrix} \quad (50B)$$

where  $\dot{\epsilon}$  is the elongation rate. One characterization of a material under this type of flow is the elongational viscosity  $\eta_e$

$$\eta_e = \frac{t(11) - t(22)}{\dot{\epsilon}} \quad (51)$$

The value of the elongational viscosity for a Newtonian liquid is three times the value of the shear viscosity. Most experimental techniques to measure  $\eta_e$  have been restricted by mechanical difficulties to the testing of high viscosity polymer melts with high shear viscosities,  $\eta_0 > 10^6$  poise, at low rates of strain,  $\dot{\epsilon} < 10^{-1} \text{ sec}^{-1}$  [22]. These restrictions do not apply to a technique which employs bubble dynamics in a non-Newtonian fluid.

Pearson and Middleman [59, 60] have experimentally observed, and theoretically analyzed, the collapse of a spherically symmetric cavity in a viscoelastic fluid. In spherical coordinates this is easily seen to be a uniaxial elongational flow and kinematic considerations lead to

$$\dot{\epsilon} = - \frac{2R^2 \dot{R}}{r^3} \quad (52)$$

in equation (50b), where the notation of section II is retained. The Rayleigh equation (4) for a general fluid becomes

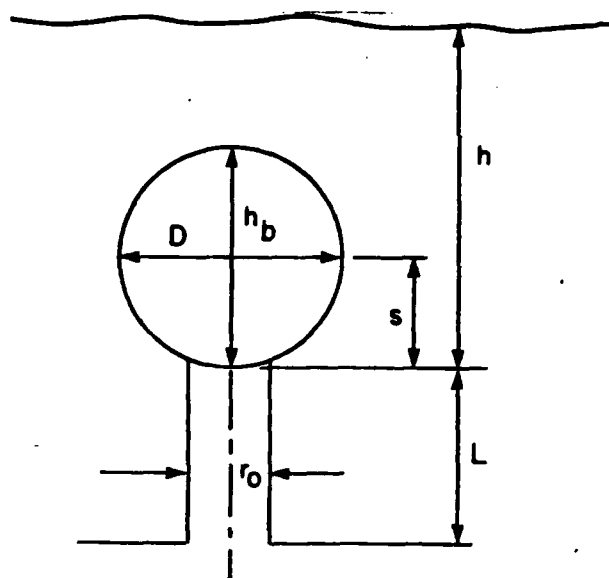
$$\rho(R\ddot{R} + \frac{3}{2}\dot{R}^2) = p(R) - p_\infty + \int_R^\infty [\underline{V} \cdot \underline{T}]_r dr \quad (53)$$

Various mathematical representations of  $\underline{T}$  can then be used to predict bubble behavior. These workers chose to analyze several models, including three-dimensional versions of the Maxwell equation (32) modified with codeformational (CD) and corotational (CR) derivatives. They attempted to approximate  $\eta$  and presented

results in terms of a "bubble pressure function,"  $\phi$ , given by

$$\phi = -(3/2) \left( p_i - \frac{2\sigma}{R} \right) \quad (54)$$

which is also expressible in terms of initial values of  $t(11)$ ,  $t(22)$  and the material constants  $\lambda$  and  $\mu$  in (32). Experimentally, the apparatus schematically represented in figure 11 was utilized and bubble behavior recorded photographically. The results for these models and experimental trials are shown graphically in figure 12 for a solution of 2.0% by weight hydroxypropylcellulose in water.

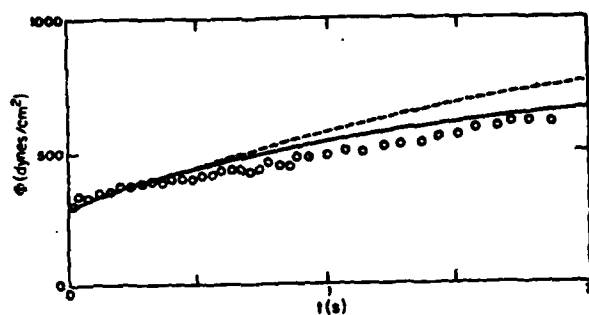


Sketch of typical experimental bubble shape showing dimensions needed for the data analysis.

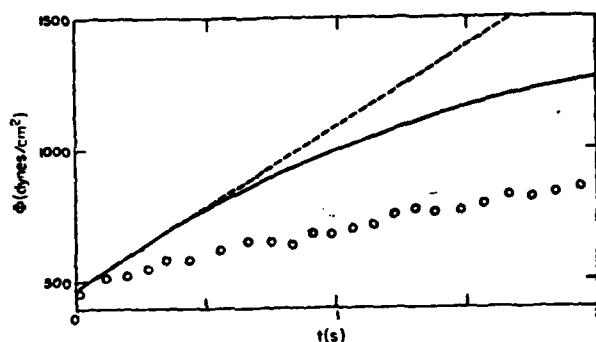
FIGURE 11 [59, P.718]

As  $\dot{\epsilon}$  increases, the agreement between theory and experiment progressively worsens. The codeformational model fails in even a gross qualitative sense for the higher elongational rates. This led to an analysis employing more complex models, including a modified corotational Maxwell fluid and an integral model, which gave much more accurate predictions.

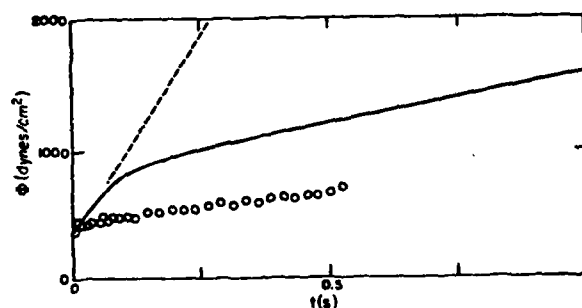
FIG. 12 [60]



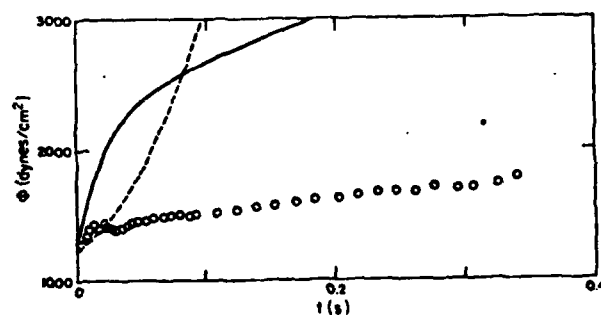
$\Phi(t)$  data compared to CD (---) and CR (—) models for bubble collapse in a HPC solution,  $\epsilon = 0.28 \text{ s}^{-1}$



$\Phi(t)$  data compared to CD (---) and CR (—) models for bubble collapse in a HPC solution,  $\epsilon = 0.58 \text{ s}^{-1}$



$\Phi(t)$  data compared to CD (---) and CR (—) models for bubble collapse in a HPC solution,  $\epsilon = 0.77 \text{ s}^{-1}$



$\Phi(t)$  data compared to CD (---) and CR (—) models for bubble collapse in a HPC solution,  $\epsilon = 1.70 \text{ s}^{-1}$

Non-Newtonian effects in a situation in which departures from sphericity become important have been analyzed by Wagner and Slattery [91] as an extension of previous work for Newtonian

droplets in a uniform Newtonian flow [79]. This particular situation involved slow flow of the fluid, which allows a perturbation technique to include inertial effects. A second perturbation was then utilized to include non-Newtonian effects. The constitutive model employed for both inner and outer fluids was the Rivlin-Ericksen fluid (43) of grade 3, defined by (55)

$$\mathbf{T} = \phi_1 \mathbf{A}_1 + \phi_2 \mathbf{A}_2 + \phi_3 \mathbf{A}_1^2 + \phi_4 \mathbf{A}_3 + \phi_5 [\mathbf{A}_1 \cdot \mathbf{A}_2 + \mathbf{A}_2 \cdot \mathbf{A}_1] + \phi_6 \text{tr}[\mathbf{A}_1^2] \mathbf{A}_1 \quad (55)$$

which is the simplest grade to exhibit both normal stresses and shear-dependent viscosity. Using matched asymptotic expansions, drop shape was found to be calculable through numerous, involved perturbation coefficients. These shapes progress from "spherical to prolate spheroidal, to ovate with large end leading and finally to a teardrop shape with extended rear" as velocity increases, figure 13. These shapes are in qualitative agreement with experimental observations. Furthermore, bubbles have been shown to be a special case included in this analysis [39].

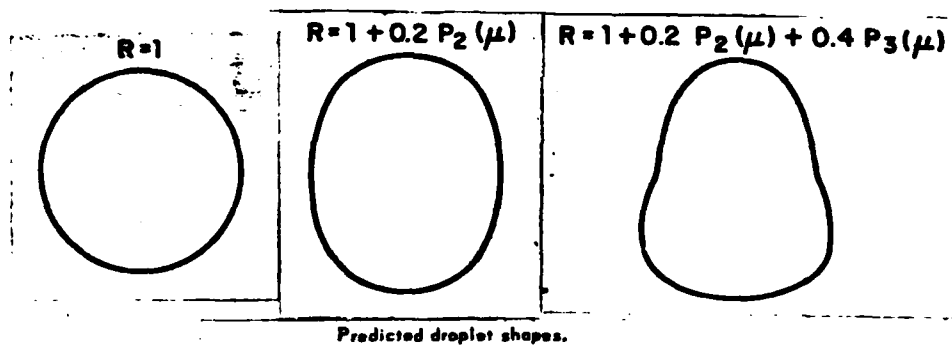


FIGURE 13 [91, P.1206]

Even an accurate constitutive equation, verified by experiment for many flows, with carefully evaluated constants, is of no value if the flow geometry of interest is too complicated to allow fruitful analysis.

Such is the case with the flows which have demonstrated the non-Newtonian effect of immediate interest, cavitation inhibition. The results of Ellis, et al. [27] are shown in figure 14 for flow past a hemispherical nose, for  $\sigma_i$ , see equation (1). Cavitation inception was measured by detection of the initial scattering of a laser which was adjusted to grazing incidence on the body. The effect was noticeable for concentrations of polyethylene oxide as low as 20 ppm, as shown in figure 15.

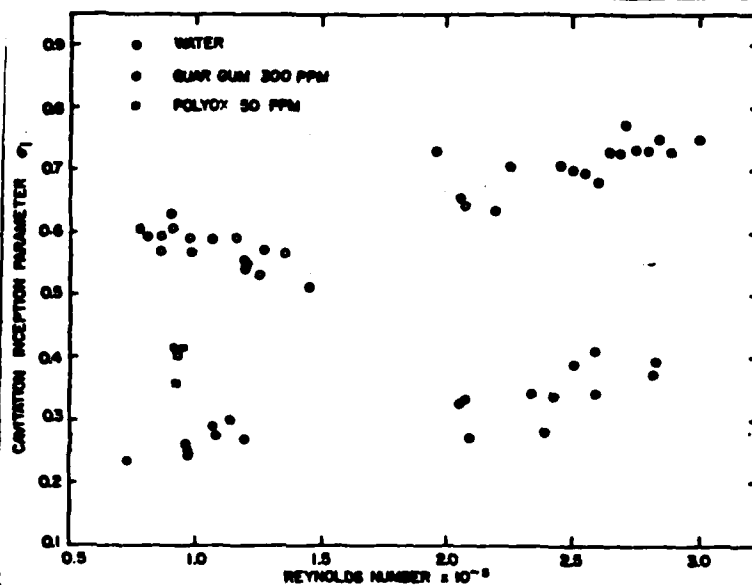
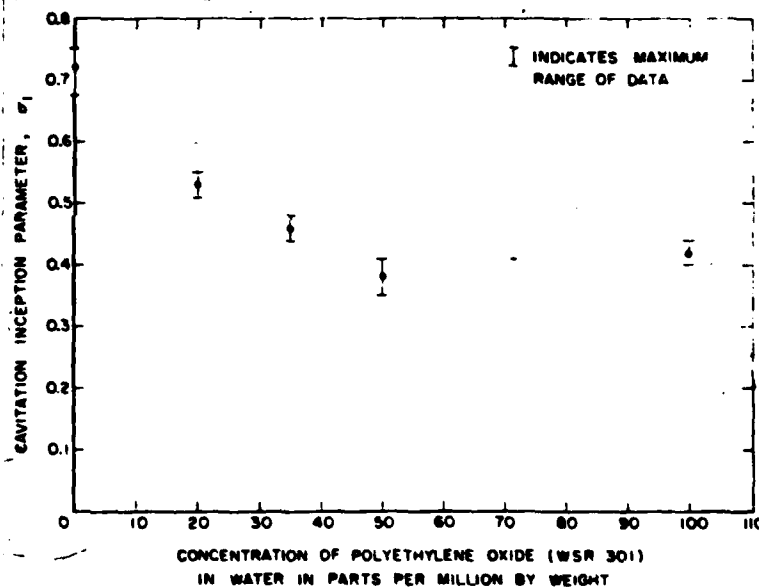
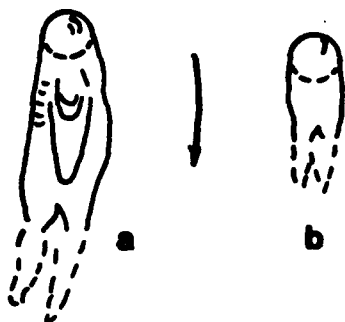


FIG. 14 & 15 [27]



The conditions under which the incipient cavitation number is strongly reduced result in another alteration in cavitation behavior which is as crucial to the complete understanding of cavitation inhibition. The appearance of the subsequent cavity is changed; the void appears smaller and clearer for the polymer solution under comparable flow conditions.



This change is noticeable for the flow past a hemispherical nose used to generate the data of figure 14, but is even more apparent for a different geometry. In figure 16 the voids created by a cylindrical cavitation inducer on a rotating disc are schematically represented for water (a) and a dilute polymer solution (b).

FIGURE 16 [83, P.900] Ting [83] takes the reduced length of the inhibited void to be an indication of a "lower cavitation intensity." He also notes:

In water, the appearance of the cavitation bubbles is very violent and chaotic, consisting of many very small bubbles. As a result it scattered much of the incipient light ... However, as the polymer is added, the cavity looks more transparent, and shows a regular, smooth wavy pattern at the vapor-liquid interface [83, P.900]

This indicates that a polymer effect is not limited to the initial stages of cavitation, and does not merely alter a mechanism of nucleation. A strong possibility exists that a single bubble should exhibit commensurate effects.

The simplest model system which might exhibit evidence of cavitation inhibition, and in the process give clues to the causes of the phenomenon, is a single bubble undergoing spherically symmetric dynamics in an otherwise quiescent fluid. Fogler and Goddard [29] may have been the first to analyze this situation for a non-Newtonian fluid. Their analysis began with equation (53), which can be transformed to

$$\ddot{R}R + \frac{3}{2}\dot{R}^2 = \frac{P_i - P_\infty}{\rho} - \frac{2\sigma}{\rho R} - (3/\rho) \int_R^\infty \frac{t_{rr}}{r} dr \quad (56)$$

A simple, linear viscoelastic constitutive equation was chosen

$$t_{rr}(t) = -2 \int_0^t N(t-t') \dot{d}_{rr}(t') dt' \quad (57)$$

and the memory function combined viscous and "Maxwellian" components as

$$M(t) = \mu \delta(t) + G_0 (-t/\lambda) \quad (58)$$

Dimensionless variables and a characteristic collapse time were defined as

$$\begin{aligned} Y &= R/R_0 & t^* &= t/t_c \\ Y_1 &= Y(t_1) & t_c &= R_0 (\rho/p_\infty)^{1/2} \end{aligned} \quad (59)$$

with the equation of motion becoming

$$\begin{aligned} \ddot{Y} + \frac{3}{2} \dot{Y}^2 &= \frac{p_0 - p_\infty}{p} - \frac{2}{N_{We} Y} - \frac{4Y}{N_{Re} Y} \\ &- \frac{12N_{e1}}{N_{Re}} \int_0^{t^*} \left\{ \exp\left[-\frac{(t^* - t_1)}{N_{De}}\right] \right\} \frac{\dot{Y} Y \ln(Y_1/Y)}{Y_1^3 - Y_1} dt_1 \end{aligned} \quad (60)$$

for initial conditions  $Y(0)=1$  and  $\dot{Y}(0)=0$ . Four dimensionless parameters arise in this equation

$$\begin{aligned} N_{De} &= \frac{\lambda}{t_c}, & \text{a Deborah number} \\ N_{El} &= \frac{G_0 t_c}{\mu}, & \text{an elastic number} \\ N_{Re} &= \frac{\rho R_0^2}{\mu t_c}, & \text{a Reynolds number} \\ N_{We} &= \frac{\rho R_0^3}{t_c \sigma}, & \text{a Weber number} \end{aligned} \quad (61)$$

By initially focusing attention on fluids with long relaxation times, corresponding to  $N_{De} \rightarrow \infty$ , the authors demonstrated a definite elastic effect on bubble collapse. For large Reynolds number the fluid approaches the limiting case of a purely elastic material and rebound short of collapse is, at least theoretically, possible. Smaller values of  $N_{Re}$  introduced viscous damping and this new mode of energy dissipation increased the value of the radius at which rebound occurred.

This work also included some calculations for finite Deborah numbers. In this case the void will eventually collapse to zero radius. However, this may not be a monotonic decrease in radius to collapse since damped oscillations may appear superposed on

the overall reduction of bubble size. A value of  $N = 0.51$  is the lower limit of this oscillatory phenomenon <sup>De</sup> for specified parameter values [ $N_{Re} = \infty$ ,  $p_0/G = 10/7$ ,  $N_{We} = \infty$ ]. Thus elasticity effects can have a pronounced influence on the behavior of a spherical cavity for  $\lambda/t = 0(1)$ .

The full explanation for cavitation inhibition is not this simple because the ratio of elastic relaxation time to characteristic collapse time in a dilute polymer solution is expected to be much less than 1. Ting [82] performed a more realistic analysis by employing a materially objective constitutive model, the Oldroyd viscoelastic fluid

$$t_{ij} + \lambda_1 \frac{D}{Dt} t_{ij} = 2\eta [d_{ij} + \lambda_2 \frac{D}{Dt} d_{ij}] \quad (62A)$$

$$\frac{D}{Dt} b_{ij} = \frac{\partial}{\partial t} b_{ij} + v_k \frac{\partial}{\partial x_k} b_{ij} + \omega_{ik} b_{kj} + \omega_{jk} b_{ki} - d_{ik} b_{kj} - d_{jk} b_{ki} \quad (62B)$$

For a dilute solution, the material constants in equation (62A) can be related to molecular and component parameters as

$$\eta = \eta_0 (1 + c[\eta]) \quad (63A)$$

$$\lambda_1 = \lambda \quad (63B)$$

$$\lambda_2 = \frac{\lambda}{1 + c[\eta]} \quad (63C)$$

$$c[\eta] < 8 \quad (63D)$$

where  $\eta$  is the solution viscosity,  $\eta_0$  is the solvent viscosity,  $\lambda$  is the terminal relaxation time of polymer molecules,  $c$  is the polymer concentration, and  $[\eta]$  is the polymer intrinsic viscosity. The mechanism by which bubble growth is triggered from the initial equilibrium radius  $R_0$  is a step change reduction in the ambient pressure of magnitude  $p^*$ . A characteristic time different from  $t_c$  defined by Fogler and Goddard (59) is employed and thermal effects, as analyzed by Plesset and Zwick [67], are included. The new dimensionless variables and characteristic time scale are given by

$$S = \frac{R}{R_0} \quad \Delta \Pi = \frac{p_2(T_0) - p_\infty(0)}{p^*} \quad (64)$$

$$\alpha = \frac{t}{t'} \quad t' = R_0 (\rho/p^*)^{1/2}$$

and the analogue to equation (60) becomes

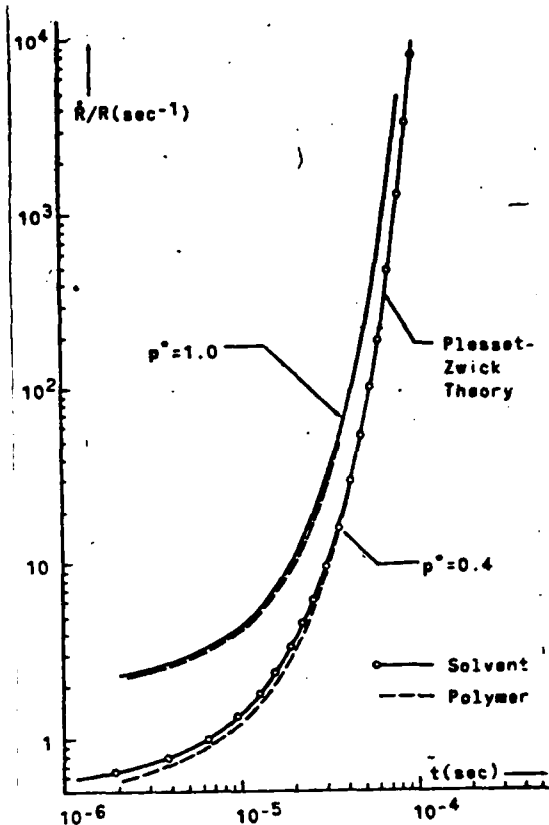
$$\begin{aligned} S\ddot{S} + \frac{3}{2}\dot{S}^2 + \frac{4}{Re} \frac{\dot{S}}{S} = \Delta\pi(1 - S^{-3\gamma}) - \frac{1}{W} S^{-1}(1 - S^{1-3\gamma}) + H(\alpha) \\ - \Phi \int_0^\alpha \frac{S^2(x) \dot{S}(x)}{[\int_x^\infty S^4(y) dy]} dx - 2E \int_0^\alpha \exp[(x-\alpha)t'/\lambda] \frac{\dot{S}(x)}{S(\alpha)} [1 + \frac{S^2(x)}{S^2(\alpha)}] dx \end{aligned} \quad (65)$$

where  $H(\alpha)$  is the Heaviside step function,  $\gamma$  is the polytropic gas exponent, and the new dimensionless parameters are

$$\begin{aligned} W &= \frac{p^* R_0}{2\sigma}, \quad \text{a Weber number} \\ \Phi &= \frac{aL\rho'}{\rho k R_0} \left(\frac{D}{W}\right)^{1/2} t'^{3/2}, \quad \text{which measures thermal effects} \\ Re &= \frac{R_0}{\eta} (p^* \rho)^{1/2}, \quad \text{a Reynolds number} \\ E &= \frac{c[\eta]\eta_0}{\lambda p^*}, \quad \text{an elastic number} \end{aligned} \quad (66)$$

Numerical calculations of  $\dot{R}/R$  vs. time were carried out for parameter values corresponding to a 500 ppm solution of polyethylene oxide ( $M_w = 4.5 \times 10^5$ ) for initial bubble size  $1.02 \times 10^{-3}$  cm and initial temperature  $T = 103^\circ \text{C}$ .

Results, figure 17, show little elastic effect. Experimental results for a similar situation [81] demonstrate a comparably small effect. The gross cavitation inhibition present in flow systems is not in evidence here. The values of  $N_{De}$  used by Fogler and Goddard, which did generate a large effect, are seen to be physically unrealistic.

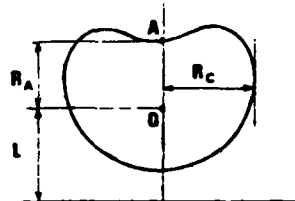


Initial bubble growth rates in the solvent and in the polymer solution.

FIGURE 17 [82, P.1430]

Since significant cavitation inhibition is not present in a spherically symmetric flow, generation and analysis of more complicated bubble geometries is indicated.

The jet-forming behavior of a collapsing bubble near a solid boundary was observed by Chahine and Fruman [14].



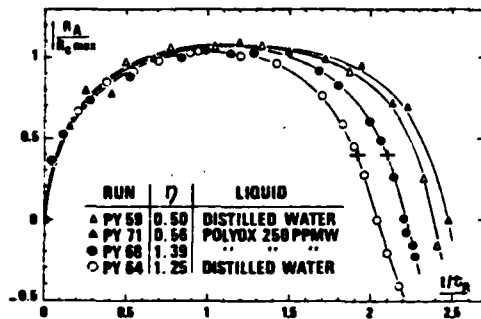
Definition of main geometric characteristics of a bubble near a solid wall.

FIGURE 18 [14, P.1406]

They defined geometric characteristics as in figure 18, and a ratio  $\eta$

$$\eta = R_{C,max} / l \quad (67)$$

The addition of polymer solute seemed to stabilize the sphericity of the cavity and to reduce the intensity of the re-entering jet in experimental trials, see figure 19.



Comparison of bubble behavior in water and Polyox solution for equivalent values of  $\eta$ .

FIGURE 19 [14, P. 1407]

Thus, although the mechanism is far from clear, it does seem that this non-Newtonian effect can be observed in single bubbles.

#### IV PRELIMINARY ANALYSES

In any attempt to find an explanation for and clarify the major factors contributing to a phenomenon as intricate as cavitation inhibition, it is necessary to obtain preliminary results. These results are expected to be first steps and half-steps toward comprehension of the techniques necessary for a complete analysis. They often ignore elements of the physical situation which are integral to the effect of interest or virtually duplicate previous work. The hope remains that a basic understanding of the importance of a given factor, by its inclusion or exclusion, will ensue.

The complete model system for this analysis consists of a cavitation bubble changing size in a non-Newtonian fluid, while this fluid experiences an imposed flow. Preliminary analyses in spherical bubble dynamics seek confirmation of previous works on the contribution of viscous, inertial, thermal, surface tension and elastic effects and clarification of the role of each. An imposed flow creates nonspherical bubbles, and artificial means may be employed to study the effect of nonsphericity alone. The imposed flow alone can also be studied, and might give some basis for choice of a useful constitutive equation. After each element of the system is examined individually, it is presumed that they can be combined in a workable analysis.

## PRELIMINARY RESULTS

### Viscosity and Inertia in Spherical Bubble Growth

Neglecting the thermal and elastic terms in Ting's analysis [89], his result (65) becomes

$$\begin{array}{cccccc} \text{(A)} & \text{(B)} & \text{(C)} & \text{(D)} & \text{(E)} & \text{(F)} \\ S\ddot{S} + \frac{3}{2}\dot{S}^2 + \frac{4}{Re}\frac{\dot{S}}{S} = \Delta\pi(1 - S^{-3\gamma}) - \frac{1}{W}S^{-1}(1 - S^{1-3\gamma}) + H(\alpha) \end{array} \quad (65')$$

where  $S(\alpha)$  is a dimensionless bubble radius which is a function of dimensionless time  $\alpha$ . The first two terms of this expression, (A) and (B), embody inertial effects, term (C) includes viscous effects, term (D) includes the internal and ambient pressure difference, term (E) takes surface tension into account and the last term, (F) arises from the step change decrease in ambient pressure of magnitude  $p^*$ , which is assumed to trigger bubble growth. (See section III for a more complete explanation.)

Ignoring the inertial terms, (A) and (B), the creeping flow expression for radius vs. time results. In real time, for all  $t > 0$ ,

$$t = - \frac{4t'}{Re} \int_{1/R_0}^{1/R} \{x[(-\Delta\pi + \frac{1}{W})x^3 + (-\frac{1}{W})x + (1.0 + \Delta\pi)]\}^{-1} dx \quad \begin{array}{l} (68A) \\ (68B) \end{array}$$

$$x = 1/R$$

There exists a critical value of the initial radius,  $R_0^c$ , which results when

$$\frac{1}{W} = \Delta\pi \quad (69A)$$

$$R_0^c = \frac{2\sigma}{p_1(T_0) - p_\infty(0)} \quad (69B)$$

Physically, this is the equilibrium radius for a cavity containing no noncondensable gas; i.e. it is the minimum physically realizable equilibrium radius for a given vapor pressure, ambient pressure and surface tension. For  $R = R_0^c$  equation (68A) can be simplified to give the time for bubble growth as

$$t = \frac{t'}{Re(1+\Delta\pi)} \ln\left[\frac{S - \Delta\pi/(1+\Delta\pi)}{1 - \Delta\pi/(1+\Delta\pi)}\right] \quad (70)$$

A more complicated general analytic solution exists for  $R > R^C$ . Calculated profiles are shown in figures 20, 21, and 22 for the physical parameters corresponding to water superheated to 103°C.

Retaining terms (A) and (B), but assuming term (C) is negligible, the result for the inviscid case is

$$t = R_o \{ \rho / [P_i(T_o) - p_\infty(0)] \}^{1/2} \int_{1/R_o}^{1/R} \left\{ \frac{2}{3}(1+W) - x + \left[ \frac{Re^2}{16W} + \frac{1}{3} - \frac{2}{3}W \right] \right\}^{-1/2} \frac{dx}{x^2} \quad (71)$$

for  $R = R^C$ . This is an elliptic integral. However, analytical results require numerous tedious transformations to arrive at standard forms, and tabular results of the subsequently required values for the three types of elliptic integrals are not readily available. Numerical integration was employed as a simple alternative to generate the profiles of figures 20, 21 and 22.

Dergarabedian's experimental results, which are expected to include thermal effects and which closely approximate the analytic results of Ting (recall Ting's analysis includes an elastic term), see figure 17, are also shown in figures 20 and 21. From the lack of agreement between these data and the theoretically generated results, it is apparent that the excluded effects are very important. Inertia also appears to be more important than viscosity in this situation.

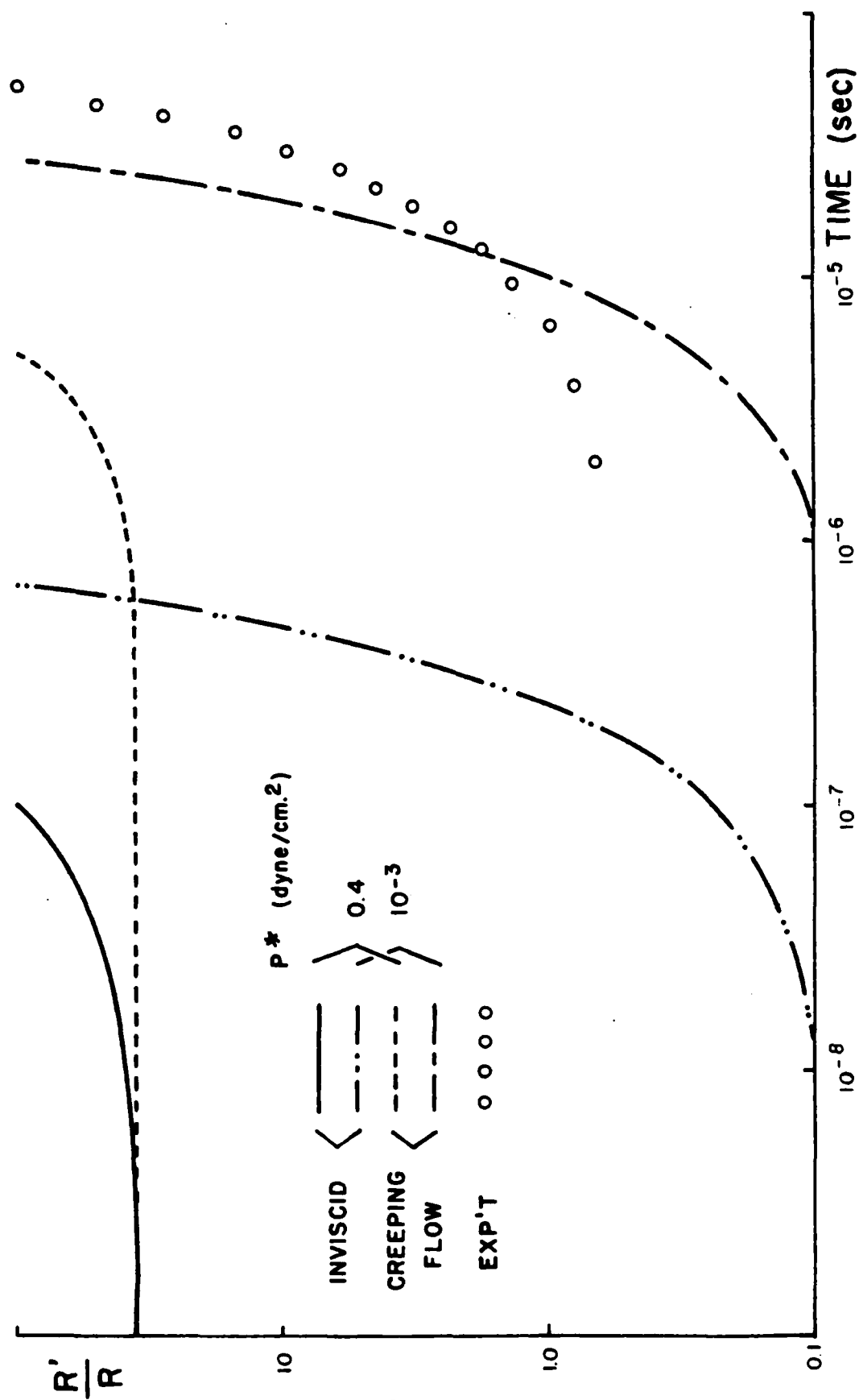


FIG. 20

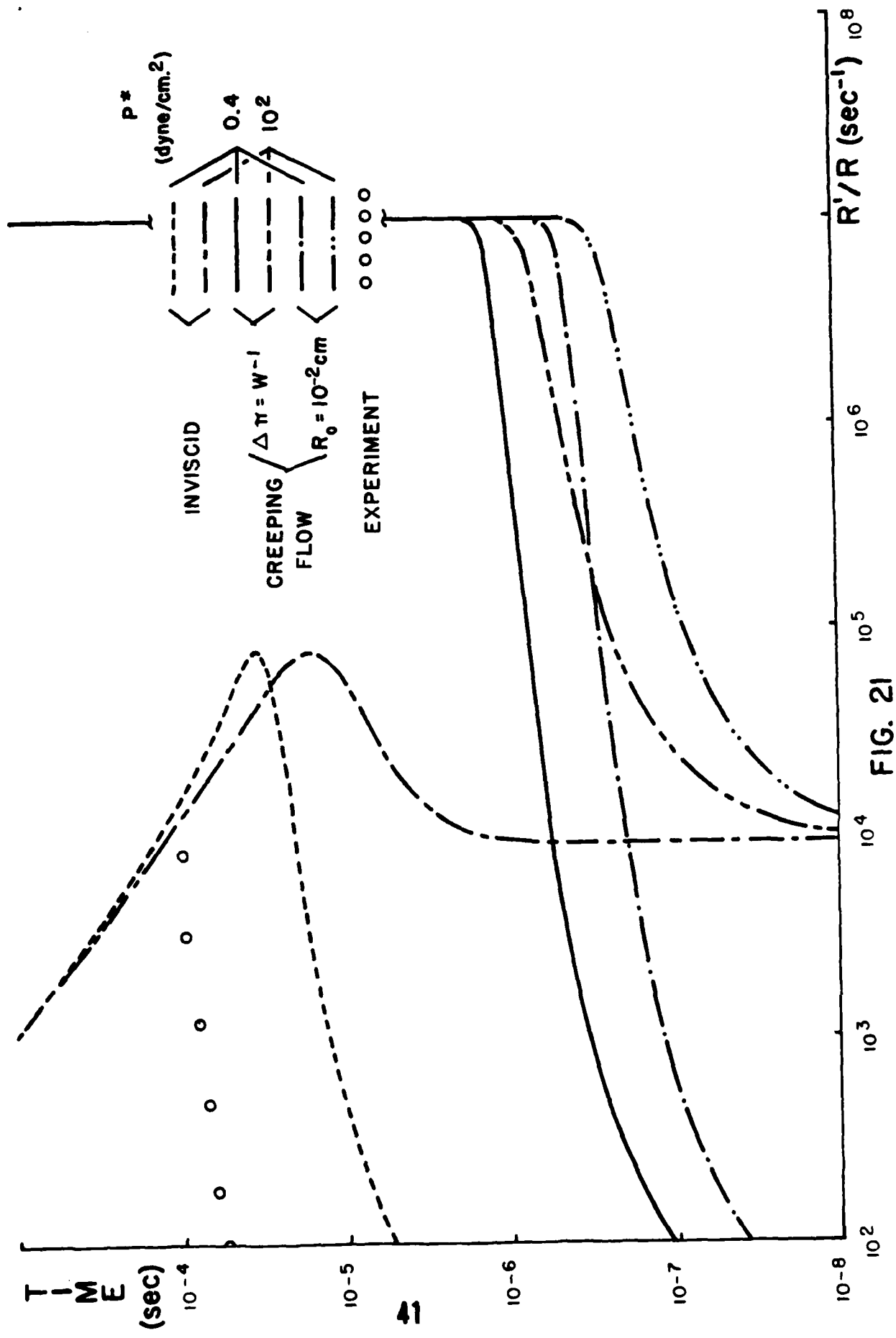


FIG. 21

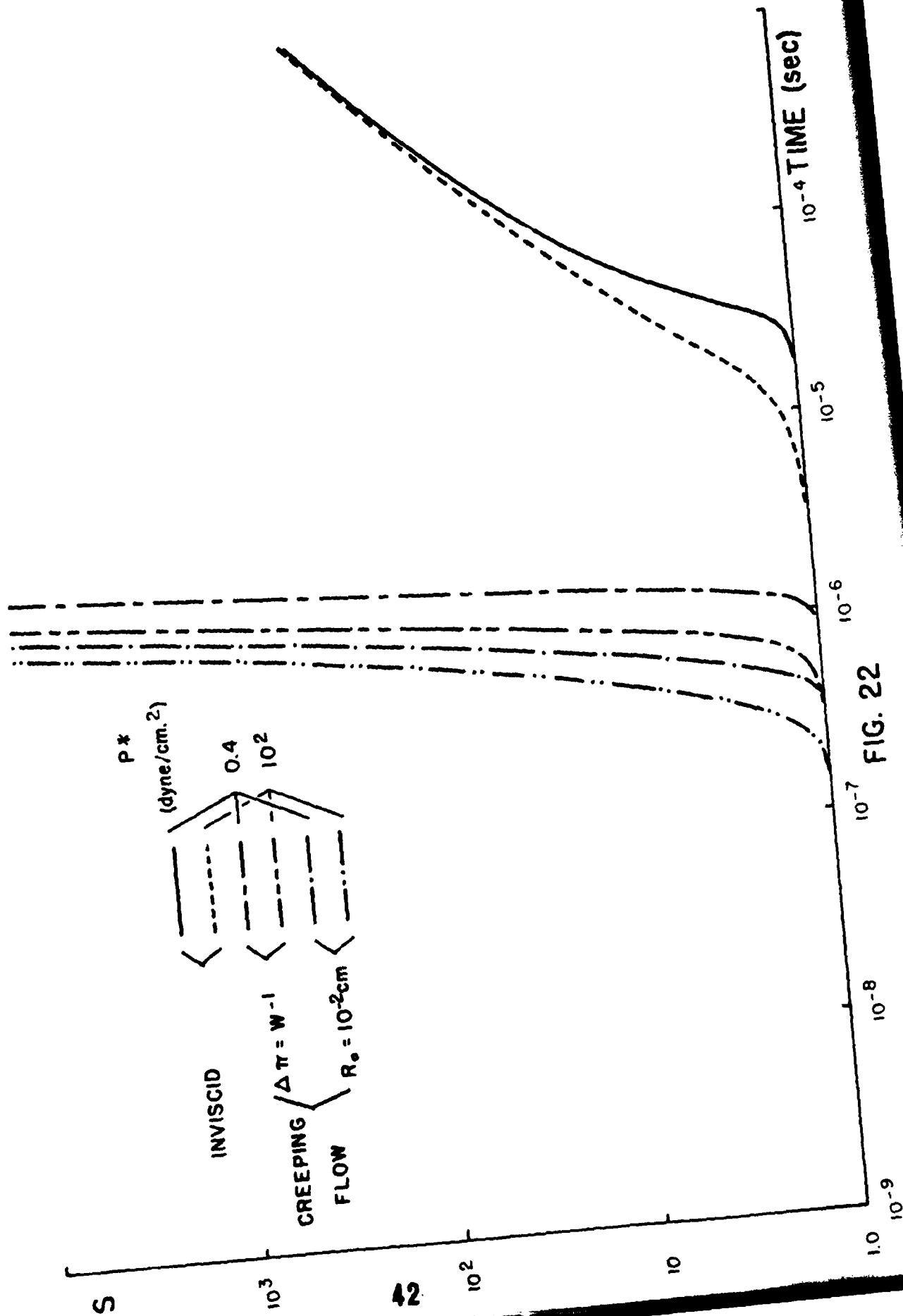


FIG. 22

### Imposed Flow

To investigate the effect of an imposed elongational flow on a spherical cavity, an attempt was made to calculate the initial deformation of this cavity in an elastic solid and also in a viscoelastic liquid. The cases considered were a cavity with constant volume, and one with a volume profile given by  $V(t)$ . The interior fluid was assumed to be inviscid, both were incompressible, and inertial effects were neglected in the equations of motion. This analysis follows the work of Pröhlich and Sack [32].

The elongational flow is assumed to be undisturbed at  $r=R$ , where  $R \gg 1$

$$u_r(R, \theta, t) = 2\dot{\epsilon}(t) R P_2(\cos \theta) \quad (72A)$$

$$u_\theta(R, \theta, t) = \dot{\epsilon}(t) R P_2'(\cos \theta) \quad (72B)$$

in spherical coordinates, where  $P_2$  is the second Legendre polynomial

The formalism of Happel and Brenner [38] can be used to generate the velocity field for a Newtonian fluid in terms of spherical harmonics. The mathematical property of Legendre polynomials

$$\int_0^\pi P_i(\theta) \sin \theta d\theta = 0, \quad i \neq 0 \quad (73)$$

means that no net change in cavity volume can result from any term in a series expansion for  $v$  except the spherically symmetric  $P_0$  term. Thus, the radial velocity at the gas-liquid interface is initially given by

$$u_r(r=a) = \dot{a}(0) \quad (74)$$

$$\dot{a}(0) = \dot{V}(0)/(4\pi a^2) \quad (75)$$

for any given volume profile.

Solving for the velocity field, temporarily ignoring the zero tangential stress condition at the surface, but requiring that

$$u_\theta(r=a) = 0 \quad (76)$$

the velocity profile exterior to the spherical body is

$$u_r = \frac{a^2}{r^2} \dot{a} + \left[ \frac{3a^6}{r^4} - \frac{5a^3}{r^2} + 2r \right] \dot{\epsilon} P_2(\cos \theta) \quad (77A)$$

$$u_\theta = \left( r - \frac{a^6}{r^4} \right) \dot{\epsilon} \left[ -\frac{d}{d\theta} P_2(\cos \theta) \right] \quad (77B)$$

Calculating the tangential stress at the surface

$$\dot{\tau}_{r\theta}(r=a) = \dot{\epsilon} \left[ -\frac{d}{d\theta} P_2(\cos \theta) \right] \neq 0 \quad (78)$$

Additional velocity components, which decay as  $r$  increases, can be superposed onto this solution of the linear equations to give a combination which satisfies the desired zero stress condition. The result becomes

$$u_r = \frac{a^2}{r^2} \dot{a} + 2\dot{\epsilon} P_2(\cos \theta) \left[ -\frac{a^3}{r^2} + r \right] \quad (79A)$$

$$u_\theta = \dot{\epsilon} \left( \frac{r}{2} \right) \frac{d}{d\theta} P_2(\cos \theta) \quad (79B)$$

this axially symmetric velocity field can be recast as a stream function given by

$$\psi = \left[ a^2 \dot{a} + (a^3 - r^3) \frac{\dot{\epsilon}}{2} \sin^2 \theta \right] \cos \theta \quad (80)$$

In dimensionless terms this becomes

$$\psi = \mu [\alpha + (1-x^3)(1-\mu^2)] \quad (80')$$

where

$$\begin{aligned} \mu &= \cos \theta \\ x &= r/a \\ \alpha &= \dot{a}/(a\dot{\epsilon}) \\ \psi &= \psi/(a^3 \dot{\epsilon}) \end{aligned} \quad (81)$$

Streamlines for various values of  $\alpha$  are shown in figures 23, 24, 25, & 26. The simplicity of this solution suggests that, at least for creeping flows, initial problems are tenable analytically. Also, the form of the solution and the streamlines confirm that the bubble will deform, and that techniques for nonspherical surfaces are necessary for subsequent work.

FIG. 23

$\alpha = 0.0$

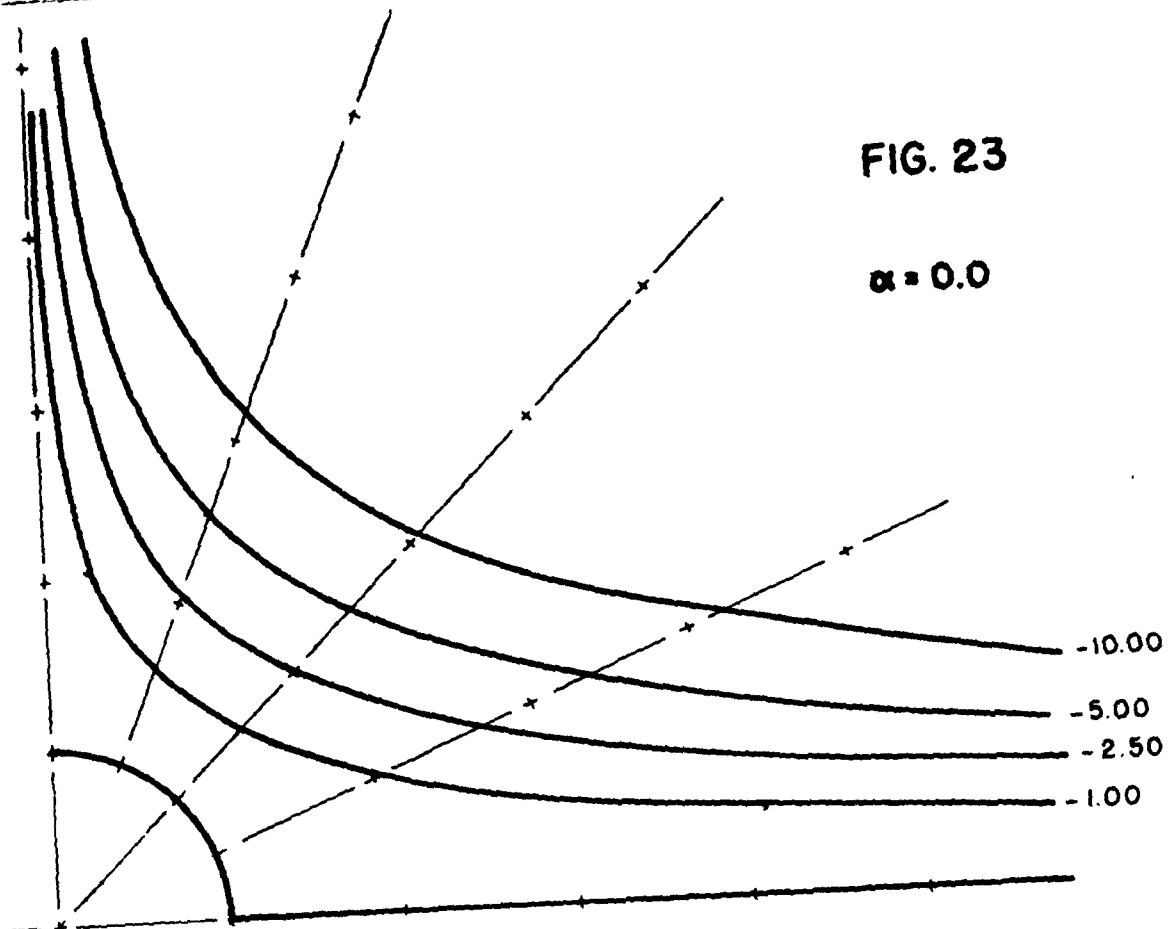


FIG. 24

$\alpha = 1.0$

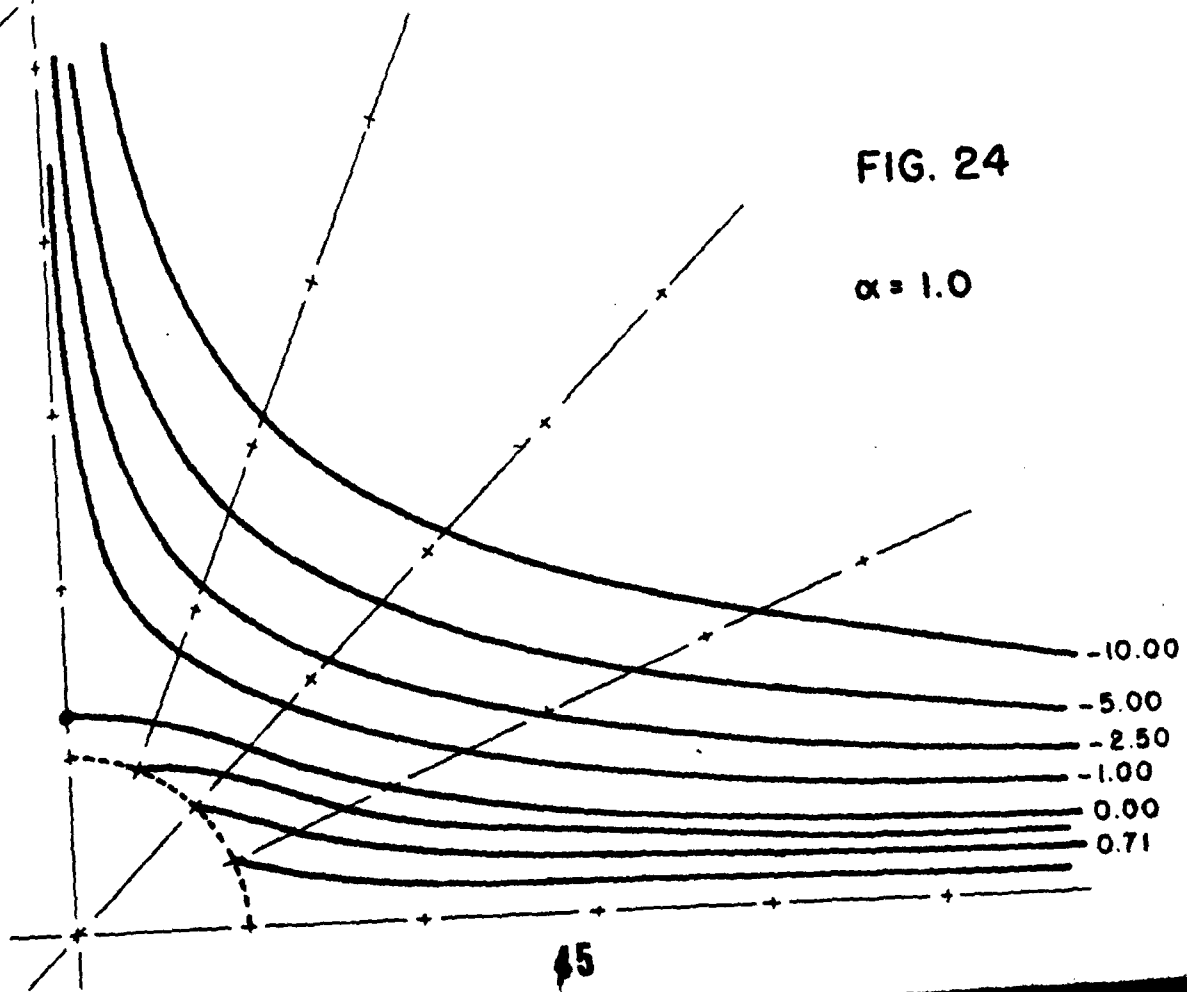


FIG. 25

$\alpha = 0.25$

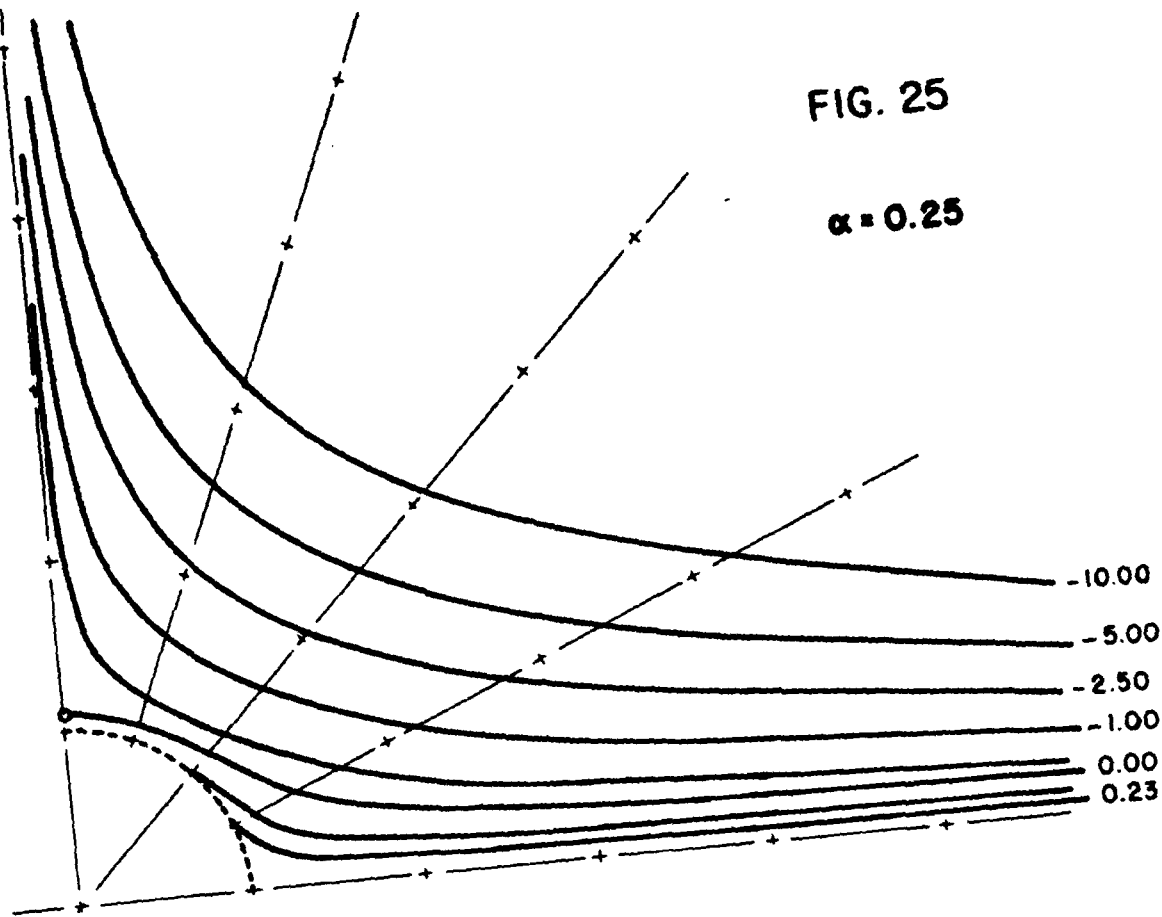
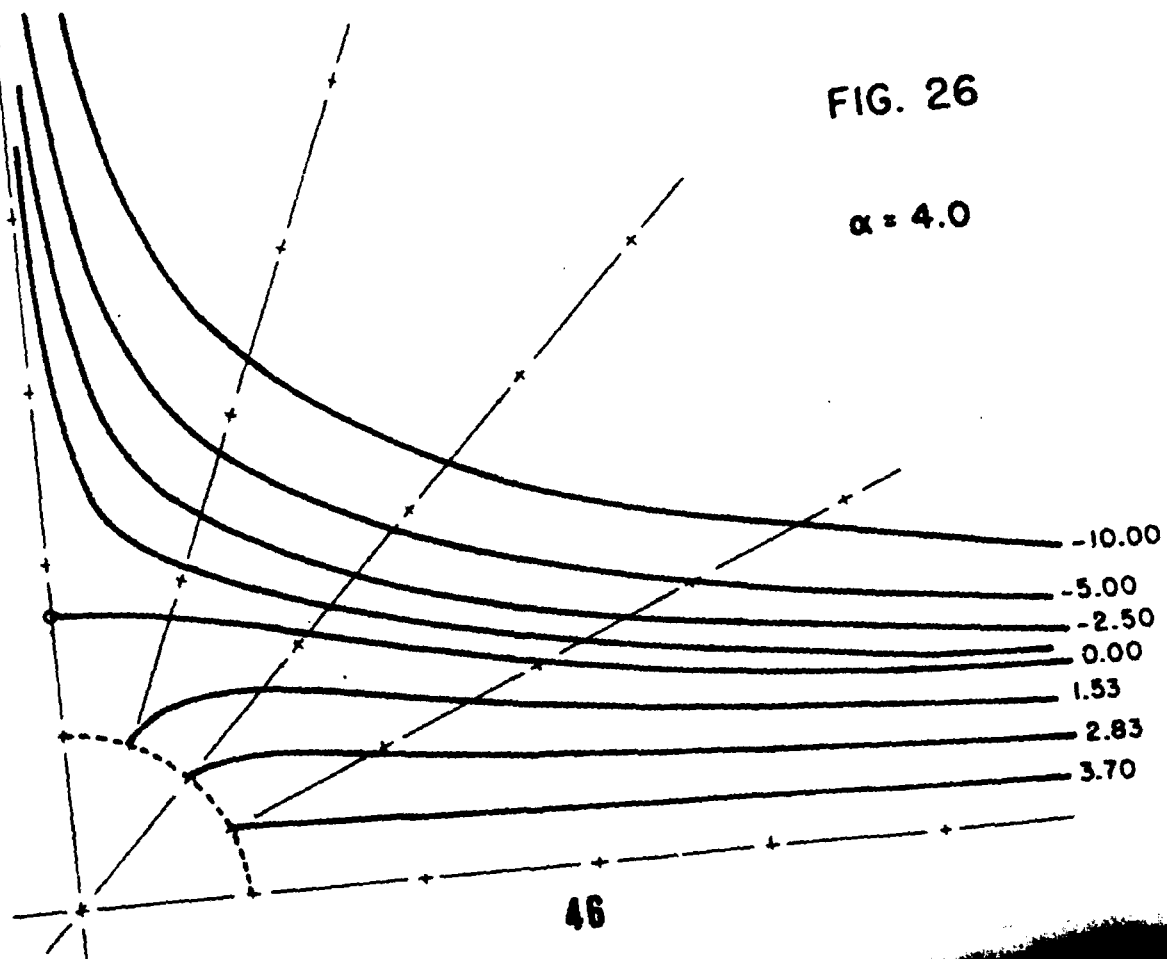


FIG. 26

$\alpha = 4.0$



### A Perturbed, Growing Cavity

The effect of nonsphericity is studied through the specification of an artificial situation. Assume an inviscid cavity is generated, with a fixed, specified shape which is a slight perturbation from a sphere. Also assume that the value of the equivalent radius of the cavity is given as a function of time, and that inertial effects are negligible in the Newtonian surrounding fluid.

Specify the shape, for small parameter  $\epsilon$ , as

$$R(t) = a(t)[1 + \epsilon f(\mu)] \quad (82A)$$

$$\max[f(\mu)] = O(1) \quad (82B)$$

$$\mu = \cos \theta \quad (82C)$$

$\eta$  = fluid viscosity

Perform a perturbation analysis

$$\underline{u} = \underline{u}^{(0)} + \epsilon \underline{u}^{(1)} + O(\epsilon^2) \quad (83A)$$

$$p = p^{(0)} + \epsilon p^{(1)} + O(\epsilon^2) \quad (83B)$$

The geometric perturbation function  $f(\mu)$  can be expanded as a summation of surface harmonics,  $P_n(\mu)$ . If a trial function  $f_1(\mu)$  is chosen

$$f_1(\mu) = P_2(\mu) \quad (84)$$

and the expansions of Cox [20] are applied, then it is easy to show that

$$\underline{u}_r = \frac{a^2}{r^2} \dot{a} + \epsilon \{ 3\dot{a} P_2(\mu) (a/r)^2 [3(a/r)^2 - 2] \} + O(\epsilon^2) \quad (85A)$$

$$\underline{u}_\theta = 0 + \epsilon \left[ 3\dot{a} \frac{a^4}{r^4} P_2'(\mu) (u-\mu^2)^{1/2} \right] + O(\epsilon^2) \quad (85B)$$

The homogeneous nature of the boundary condition applied at the surface, zero tangential stress, means that this velocity profile is also valid for a linear viscoelastic fluid. Again, as in the previous result, the creeping flow problem has been shown to be straightforward and amenable to a perturbation analysis.

## PROPOSED PRELIMINARY ANALYSES

### Elasticity, Surface Tension and Thermal Effects

The result of Fogler and Goddard, equation (60), and of Ting, equation (65), can be solved for more parameter values to generate profiles like those in figures 20, 21 and 22. With carefully chosen values for these physical constants, i.e. systematic departures from the values expected for pure water, dilute polymer effects on spherically symmetric growth are expected to be demonstrated to be minimal.

### Imposed Flow

First, the analyses in the preliminary results section under this subheading require completion. In addition, the initial deformation of a spherical cavity under other imposed flows, such as simple shear or the combination of shear and vorticity afforded by an orthogonal rheometer, can be calculated. The stress field should also be evaluated with particular attention paid to changes in the magnitude of normal stresses. These attempts should employ various constitutive relations, with parameters corresponding to liquids ranging from a purely viscous, to a completely elastic material.

## V ULTIMATE PLANS and GOALS for this Research

The preferred goal of this research is to determine, by means of theory and experiment, whether a model system consisting of a single bubble in a well-characterized non-Newtonian flow exhibits the gross effects of cavitation inhibition.

### THEORETICAL

Most of the preceding pages have been devoted to an introduction to the approaches and techniques available for theoretical analysis of a bubble system. At this stage, it is impossible to predict which single technique will be most important. All will probably become necessary.

However it is achieved, the resultant theoretical system should be flexible and capable of including various flow configurations. This is expected to allow some evaluation of the importance of various factors within a flow, such as vorticity and shear rate. A procedure which may be particularly important is a search for an imposed flow which allows a steady state nonspherical shape of a bubble with constant internal pressure. The existence of such a flow is suggested by the first special case mentioned by Rallison [71], the "weak flow" conditions. For a bubble, the viscosity ratio  $\lambda$  (23a) is very small, so the requisite flow strength for equilibrium might be too low to generate important nonspherical effects. If this is not the case, it is possible that the change in cavitation intensity noted by Ting [82] will be manifest in a change of shape and/or volume of the steady state cavity. This is likely to be a much simpler analysis than any including bubble growth, especially if ellipsoidal harmonics are applicable.

Just as Pearson and Middleman's analysis gives some basis for the evaluation of constitutive relations, the results here may be of value in the assessment of constitutive accuracy. Even without experimental results for comparison, physically unreasonable results may eliminate certain equations. With experimental data, still closer scrutiny should be possible.

The problems expected here are numerous, particularly since

the nonlinearity of the complete equations of motion makes analytic solutions unlikely. Exact solutions for limiting cases will be found whenever possible, and the need for a great deal of effort and cleverness is anticipated in order to generate numerical solutions.

#### EXPERIMENTAL

Two major types of experiments are envisioned in plans for this research: **exploratory** and **confirmatory**. Exploratory experimentation is conducted concurrent with theoretical work. Its purpose is to guide the development of theory, eliminating unimportant approaches and distinguishing physical effects from purely mathematical ones. From this initial type of experimental work and theoretical analysis, a full theoretical model should arise, and final testing and adjustment is made through "confirmatory" experimental trials.

Before any of this work begins, logistical and technical problems must be solved or circumvented. These include choice of materials and apparatus, procurement of funds, and even ordering and delivery constraints. Once the apparatus is assembled, techniques must be learned and honed, and trial runs conducted. A long process is expected to precede any experiments which approach the model system. Initial decisions concerning apparatus will depend on preliminary analyses and past work for guidelines. Careful choice and characterization of fluids must be made, then means must be devised for flow generation, bubble generation, and the recording and analysis of bubble behavior.

The reference fluid will, of course, be water, while the test fluids are expected to be dilute solutions of polymers such as polyethylene oxide [14, 27], guar gum [27], or polyacrylamide [15, 83]. The choice will depend upon the behavior of candidate additives under some new conditions which may be present in the experimental procedure. All fluids must be characterized viscometrically, and also checked for variations in physical parameters, such as surface tension, from the values for pure water. The flow apparatus used to generate the imposed flow may

also be useful for fluid characterization.

The specific machinery necessary for flow generation will of course depend on the desired flow. A simple one-dimensional shear flow can be generated by a two-belt apparatus (see figure 27a). A two-dimensional extensional flow results from a four-belt apparatus (see figure 27b). A Couette flow can easily be generated experimentally (see figure 27c). Perhaps the most flexible, single flow geometry is present in an orthogonal rheometer (figure 27d). By varying the offset, rotation rate and plate gap, the amount of vorticity and shear present in the undisturbed flow can be varied independently. Hakimi and Schowalter [37] used just such a device in their experiments with drop deformation. Thus the technology for and components of a unit should be available in the Princeton University Department of Chemical Engineering, where this research is being conducted.

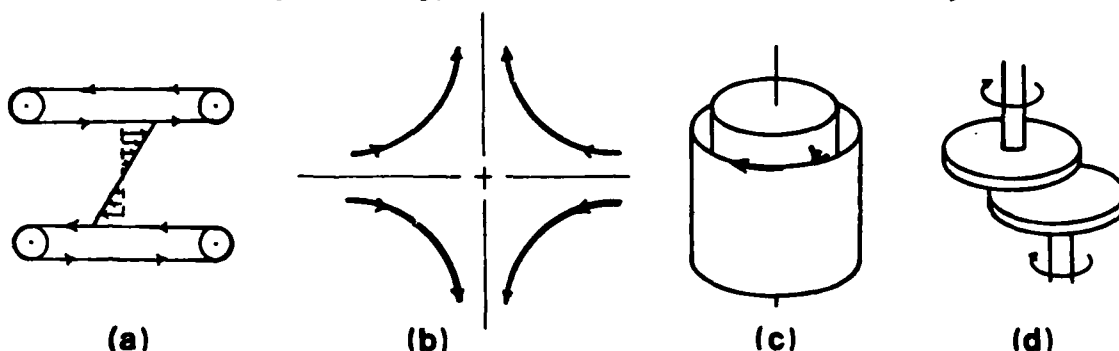


FIGURE 27 Possible Experimental Flow Apparatus

The most versatile and sophisticated of the devices which may be applicable to flow generation, and will definitely be the major means of rheological characterization, is a RHEOMETRICS Mechanical Spectrometer, which is now under order by this department. Several flow geometries are available in this device, including Couette flow and orthogonal rheometer flow, with a wide range of operating parameters. This instrument has the added advantage of capability for making sensitive dynamic measurements of macroscopic elastic effects such as the total normal force on a rheometer plate. By comparing these measurements for identical imposed flows, with and without a cavity present, additional conclusions with respect to concepts

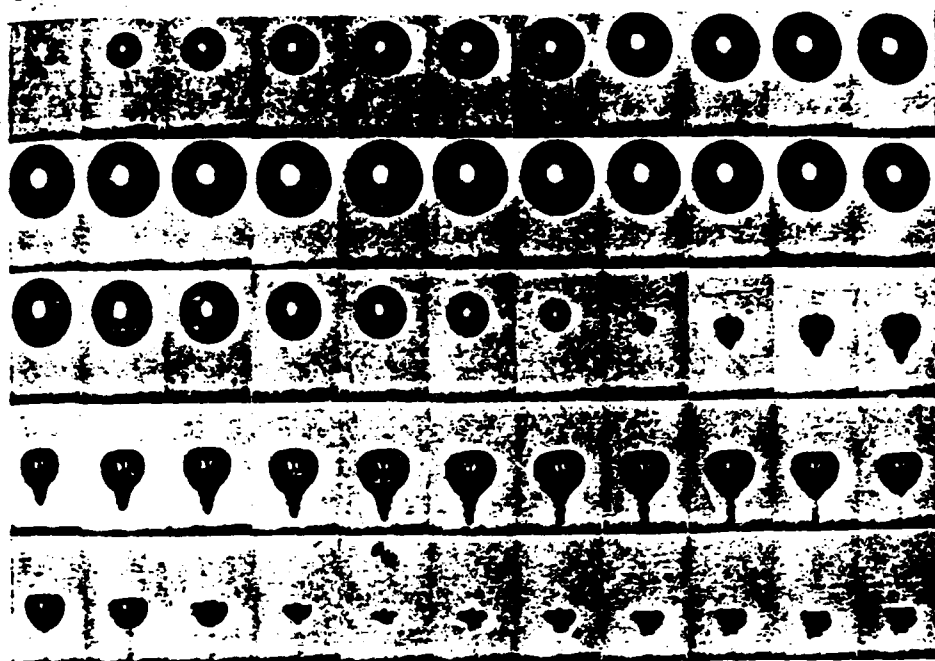
such as flow alteration may be possible.

Bubble generation can take on two levels of sophistication. If a steady state bubble shape is found to be achievable, then cavity formation for such a flow may be as simple as injection of a measured volume of vapor or gas into the static fluid.

To produce cavitation bubbles for dynamic study the technique with the largest probability of success is the use of a laser to trigger nucleation. A Q-switched ruby laser has been used to successfully generate volumes in pure water which are well-modelled as single cavitation bubbles [52, 53]. The Q-switch is a shutter which contracts the pulses of the ruby laser into smaller segments of length 30-50 nsec. In this short time, about 1 J of energy is introduced into a small region of the fluid. Available references on lasers [51] show a wide variety of similar devices to be evaluated.

The recording system is also very different for the steady state or dynamic bubble. The steady state shape requires only single photographs of two or three views of the bubble. With adequate lighting, a simple Polaroid camera should suffice, although slide capability would be desired to allow projection of the images.

The dynamic bubbles are expected to change on a time scale of about  $10^{-5}$  sec. or less (figures 20 and 21). Recording of such rapid events photographically requires a very high framing rate. Cameras with rates this high, and higher, are available [75], and have been used to record bubble dynamics (figure 28). These cameras, however, are extremely expensive, e.g. the Cordin 330 with framing rate of  $2 \times 10^6$  pictures per second costs approximately \$100,000. Rental of such units is also available. This is an attractive proposition, especially for the early trials when needs are not completely known. If the flow is not axisymmetric, more than one view of a bubble will be necessary for analysis. Should reproducibility be found to be excellent, then photography of the different views in different trials will be acceptable; if not, an optical system for recording multiple images on one frame may be necessary.

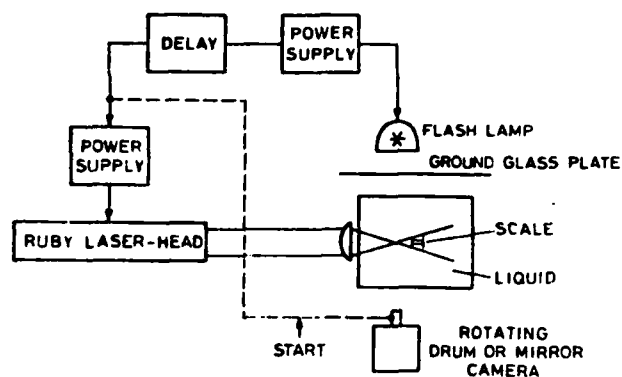


Dynamics of a laser-produced spherical bubble near a solid boundary. The framing rate is 75000 frames/s, the maximum bubble radius  $R_{\max} = 2.0$  mm, the distance of the bubble centre from the boundary  $l = 4.9$  mm and the size of the individual frames is  $7.2 \times 4.6$  mm.

FIGURE 28 [53, P.400]

Analysis of the massive photographic record anticipated will probably require countless projections of individual images, and subsequent fitting to analytical expansions. Fortunately, exploratory trials will probably be most useful for qualitative results, reducing the need for exhaustive examination of the images. Later, a good theoretical model will give accurate predictions, minimizing the deviation from predicted shapes and the need for fitting.

The proposed overall system is diagrammatically presented in figure 29. Of course, the details are dependent upon future developments.



Block diagram of experimental setup.

FIGURE 29 [52, P.23]

Many unforeseeable problems are expected to arise in the course of this work. Others may be at least partially anticipated and must be resolved for success to be achieved. Possible problems include:

1) Multiple bubbles

The ruby laser is thought to cause nucleation on dust particles [77]. The polymer solute molecules may act as nucleating centers, the result being formation of multiple bubbles. A possible solution would be to split the laser and to focus multiple beams on a single point from many angles.

2) Polymer degradation

The laser may also cause thermal degradation of polymer. This is very likely, at least in the immediate vicinity of the focal point, and must be evaluated for macroscopic effect.

3) Surface tension

Impurities in water are thought to change the dynamics of a single bubble in Stokes flow by altering surface tension. Polymer molecules might cause a similar phenomenon.

4) Vapor pressure

Is the vapor pressure of a dilute solution the same as that of the solvent? Measurements need to be taken here. One possibility for testing the coupled effects of 3) and 4) is a static bubble comparison between water and the solution, since surface tension and vapor pressure are the major determinants of

equilibrium radius.

5) Thermal effects

Error may be introduced into the system by a change in thermal properties of the liquid or laser heating effects. Heat effects from photographic lighting can be minimized using proper filters.

6) Wall effects

By varying apparatus or bubble dimensions, it should be possible to estimate the effects of the finite extent of the experimental fluid. In using the Mechanical Spectrometer, normal force readings may also give an indication of the difference between theoretical flows imposed at infinity and real flows.

## VI BIBLIOGRAPHY

1. Acosta, A.J. & B.R. Parkin J Ship Res 19 193-203 (1975)  
Cavitation - A Selective Review
2. Acrivos, A. & T.D. Taylor CES 19 445-451 (1964)  
The Stokes Flow past an Arbitrary Particle:  
The Slightly Deformed Sphere
3. Alexander, D.E. & A.C. Messer McGraw-Hill 1972 91Pp  
Fortran IV Pocket Handbook
4. Barthes-Biesel, D. & A. Acrivos JFM 61 1-21 (1973)  
Deformation and Burst of a Liquid Droplet Freely  
Suspended in a Linear Shear Field
5. Batchelor, G.K. JFM 41 545-570 (1970)  
The Stress System in a Suspension of Force-Free Particles
6. ----- JFM 44 419-440 (1970)  
Slender Body Theory for Particles of Arbitrary  
Cross-Section in Stokes Flow
7. ----- JFM 46 813-829 (1971)  
The Stress Generated in a Non-dilute Suspension of  
Elongated Particles by Pure Straining Motion
8. Bird, R.B., R.C. Armstrong & O. Hassager Wiley 1977 470Pp  
Dynamics of Polymeric Liquids  
Volume I: Fluid Mechanics
9. Bird, R.B. & S.I. Abdul-Khalik  
AICHEJ 20 1041-1066 (1974)  
Co-Rotational Rheological Models and the Goddard Expansion
10. Blake, J.R. Proc Cambridge Phil Soc 70 303-310 (1970)  
A Note on the Image System for a Stokeslet  
in a No-slip boundary
11. Blake, J.R. & A.T. Chwang  
Fundamental Singularities of Viscous Flow  
Part I: The image systems in the vicinity of a  
stationary no-slip boundary  
J Eng Math 8 23-29 (1974)  
Part II: Applications to slender body theory  
J Eng Math 8 113-124 (1974)
12. Brewer, F.G. & K.F. Rieckhoff  
Phys Rev Letters 13 (11) 334a-336a (1964)  
Stimulated Brillouin Scattering in Liquids
13. Burgers, J.M. Kon. Ned. Akad. Wet. Verhand.  
(Eerste Sectie) D1 XVI No.4 (1933)  
pp 1-287 Amsterdam Noord-Hollandsche  
"Second Report on Viscosity and Plasticity"
14. Chahine, G.L. & D.H. Fruman  
Phys Fluids 22 1406-1407 (1977)  
Dilute Polymer Solution Effects on Bubble Growth  
and Collapse
15. Chang, C-P Princeton Oct 1975  
Thesis: Secondary Flow Induced by a Cylinder  
Oscillating in a Viscoelastic Liquid
16. Chang, C-P & W.R. Schowalter Nature 252 686-688 (1974)  
Flow near an Oscillating Cylinder  
in Dilute Viscoelastic Fluid

17. Chapman, R.B. & M.S. Plesset J Basic Eng D94 142-146  
Nonlinear Effects in the Collapse of a Nearly Spherical  
Cavity in a Liquid
18. Chwang, A.T. & T.Y. Wu  
Hydromechanics of Low Reynolds Number Flow  
Part 1: Rotation of Axisymmetric Prolate Bodies  
JFM 63 607-622 (1974)  
Part 2: Singularity Method for Stokes Flow  
JFM 67 787-815 (1975)  
Part 3: Motion of a Spherical Particle  
in Quadratic Flows  
JFM 72 17-34 (1975)  
Part 4: Translation of Spheroids  
JFM 75 677-689 (1975)
19. Cole, R.H. Dover 1948 437Pp  
Underwater Explosions
20. Cox, R.G. JFM 37 601-623 (1969)  
The Deformation of a Drop in a General Time-Dependent  
Fluid Flow
21. -----  
The Motion of Long Slender Bodies in a Viscous Fluid  
Part 1: General Theory  
JFM 44 791-810 (1970)  
Part 2: Shear Flow  
JFM 45 625-657 (1971)
22. Dealy, J.M. Polym Eng Sci 11 433-445 (1971)  
Extensional Flow of Non-Newtonian Fluids - A Review
23. Dergarabedian, P. J App Mech 20 537-545 (1953)  
The Rate of Growth of Vapor Bubbles in Superheated Water
24. Einstein, A.  
A New Determination of Molecular Dimensions  
in "Investigations on the Theory of the  
Brownian Movement  
ed by P. Furth Dover 1956
25. Ellis, A.T. & J.W. Hoyt ASME 1968 Cavitation Forum p 2-3  
Some Effects of Macromolecules on Cavitation Inception
26. Ellis, A.T. & R.Y. Ting  
Non-Newtonian Effects on Flow Generated Cavitation  
in a Pressure Field  
in "Fluid Mechanics, Acoustics and Design  
of Turbomachinery"  
NASA-SP-304 pt 1 403-421 (1974)
27. Ellis, A.T., J.G. Waugh & R.Y. Ting  
J Basic Eng 3D 450 (1970)  
Cavitation Suppression and Stress Effects in High-Speed  
Flows of Water with Dilute Macromolecular Additives
28. Epstein, P.F. & M.S. Plesset  
J Chem Phys 18 1505 (1950)  
On the Stability of Gas Bubbles in Liquid-Gas Solutions
29. Fogler, H.S. & J.D. Goddard  
Phys Fluids 13 1135-1141 (1970)  
Collapse of Spherical Cavities in Viscoelastic Fluids
30. ----- J App Phys 42 259-263 (1971)  
Oscillations of a Gas Bubble in Viscoelastic Liquids Subject  
to Acoustic and Impulsive Pressure Variations

31. Frankel, N.A. & A. Acrivos JFM 44 65-78 (1970)  
The Constitutive Equation for a Dilute Emulsion
32. Fröhlich, H. & R. Sack  
PRS (London) A185 415-430 (1946)  
Theory of the Rheological Properties of Dispersions
33. Goddard, J.D. & C. Miller JFM 28 657-673 (1967)  
Nonlinear Effects in the Rheology of Dilute Suspensions
34. Golden, J.T. Prentice-Hall 1965 270pp  
Fortran IV: Programming & Computing
35. Goldsmith, H.L. & S.G. Mason  
The Microrheology of Suspensions  
pp 86-230, chapt 2  
in "Rheology: Theory & Application"  
Vol 4 ed by F.R. Eirich  
Academic Press 1967
36. Hakimi, F.S. Princeton Feb. 1976  
Thesis: The Effects of Shear and Viscosity on the  
Deformation of a Drop
37. Hakimi, F.S. & W.R. Schowalter  
JFM 98 632-645 (1980)  
The Effect of Shear and Vorticity  
on Deformation of a Drop
38. Happel, J. & H. Brenner Prentice-Hall 1965  
Noordhoff International 1973  
Low Reynolds Number Hydrodynamics  
with special application to particulate media
39. Hassager, O.  
Bubble Motion in Structurally Complex Fluids  
In "Chemical Engineering with Per. Søltøff"  
ed by K. Østergaard & Aa. Fredenslund  
Teknisk Forlag., Copenhagen 1977
40. ----- Nature 279 5712 402-3 (1979)  
Negative Wake behind Bubbles in non-Newtonian Liquids
41. Hermes, R.A. & A.G. Fredrickson  
AIChEJ 13 253-259 (1967)  
Flow of Viscoelastic Fluids past a Flat Plate
42. Hobson, E.W. Chelsea 1955 500pp  
The Theory of Spherical & Ellipsoidal Harmonics
43. Hoyt, J.W. J Fluid Eng 98 106-112 (1976)  
Effect of Polymer Additives on Jet Cavitation
44. Hsieh, D.Y. J Basic Eng 87 991-1005 (1965)  
Some Analytical Aspects of Bubble Dynamics
45. ----- J Basic Eng 94 655-665 (1974)  
On the Dynamics of Nonspherical Bubbles
46. Ince, E.L. Dover 1926 558pp  
Ordinary Differential Equations
47. Jeffery, G.B. PPS A102 161-179 (1922)  
The Motion of Ellipsoidal Particles  
Immersed in a Viscous Fluid
48. Johnson, E.D. & S. Middleman  
Polymer Eng & Sci 18 963-968 (1978)  
Elongational Flow of Polymer Melts

49. Ladyzhenskaya, O.A. Gordon & Breach, London 1963  
The Mathematical Theory of Viscous Incompressible Flow
50. Lamb, Sir Horace Dover 1945 738Pp  
Hydrodynamics
51. Laser Focus  
1979 Buyer's Guide with Fiber Optic Communication  
January, 14th ed
52. Lauterborn, W. App Phys Letters 21 27-29 (1972)  
High-speed Photography of Laser-induced  
Breakdown in Liquids
53. Lauterborn, W. & H. Bolle JFM 72 391-399 (1975)  
Experimental Investigations of Cavitation Bubble Collapse  
in the Neighborhood of a Solid Boundary
54. MacRobert, T.M. Dover 1948 372Pp  
Spherical Harmonics
55. Noll, W. Arch Rat Mech Anal 2 197-226 (1958)  
A Mathematical Theory of the Mechanical Behavior  
of Continuous Media
56. Oldroyd, J.G. PFS (London) A200 523-541 (1950)  
On the Formulation of Rheological Equations of State
57. Pearson, G.H. U. Mass Sept 1975  
Thesis: Elongational Flow of Polymer Solutions
58. Pearson, G.H. & S. Middleman CES 29 1051-1053 (1974)  
Comments on a New Method for Determination of Surface  
Tension of Viscous Fluids
59. ----- AICHEJ 23 (1977)  
Elongational Flow Behavior of Viscoelastic Liquids:  
Part I 714-721  
Part II 721-725
60. ----- Rheo Acta 17 500-510 (1978)  
Elongational Flow Behavior of Viscoelastic Liquids:  
Modelling Bubble Dynamics with  
Viscoelastic Constitutive Relations
61. Plesset, M.S. J App Phys 25 96-98 (1954)  
On the Stability of Fluid Flows with Spherical Symmetry
62. ----- Bubble Dynamics  
In "Cavitation in Real Fluids"  
ed by R. Davies Elsevier 1964
63. Plesset, M.S. & R.R. Chapman JFM 47 283-290 (1971)  
Collapse of an Initially Spherical Vapour Cavity in the  
Neighborhood of a Solid Boundary
64. Plesset, M.S. & T.P. Mitchell  
Q App Math 13 419-430 (1956)  
On the Stability of the Spherical Shape of a Vapor Cavity
65. Plesset, M.S. & A. Prosperetti  
Bubble Dynamics and Cavitation  
in "Annual Review of Fluid Mechanics"  
Vol 9 1977 Pp 145-186
66. Plesset, M.S. & S.A. Zwick J App Phys 23 95-98 (1952)  
A Non-steady Heat Diffusion Problem with Spherical Symmetry
67. ----- J App Phys 25 493-500 (1954)  
The Growth of Vapor Bubbles in Superheated Liquids

68. Prosperetti, A. Q App Math 34 339-352  
Viscous Effects on Perturbed Spherical Flows
69. ----- JFM 85 349-368 (1978)  
Vapour Bubble Growth in a Superheated Liquid
70. Prosperetti, A. & G. Seminara  
Phys Fluids 21 1465 (1978)  
Linear Stability of a Growing or Collapsing Bubble  
in a Slightly Viscous Liquid
71. Rallison, J.M.  
to appear in JFM 98 000-000 (1980)  
Time-dependent drop deformations for small deviations  
from sphericity
72. Rayleigh Philos Mag 34 94-98 (1917)  
On the Pressure developed in a Liquid during the Collapse  
of a Spherical Cavity
73. Rivlin, R.S. & J.L. Ericksen  
J Rat Mech Anal 4 323-425 (1955)  
Stress - Deformation Relations for Isotropic Materials
74. Schowalter, W.P. Pergamon 1978 300pp  
Mechanics of Non-Newtonian Fluids
75. -----  
Research Proposal (submitted to U.S. Office  
of Naval Research)
76. Scriven, L.E. CES 12 98-108 (1960)  
Dynamics of a Fluid-Interface
77. Stamberg, R.C. & D.E. Gillespie  
J App Phys 37 459-460 (1966)  
Laser-Stimulated Nucleation in a Bubble Chamber
78. Taylor, G.I. PRS A146 501 (1934)  
The formation of emulsions in definable fields of flow
79. Taylor, T.D. & A. Acrivos JFM 18 466-476 (1964)  
On the Deformation and Drag of a Falling Viscous Drop  
at Low Reynolds Number
80. Tillett, J.P.K. JFM 44 401-417 (1970)  
Axial and Transverse Stokes Flow Past  
Slender Axisymmetric Bodies
81. Ting, R.Y. AIChEJ 21 810-813 (1975)  
Viscoelastic Effect of Polymers on Single Bubble Dynamics
82. ----- Phys Fluids 20 1427-1431 (1977)  
Effect of Polymer Viscoelasticity on the Initial Growth of  
a Vapor Bubble from Gas Nuclei
83. ----- Phys Fluids 21 898-901 (1978)  
Characteristics of Flow Cavitation in Dilute Solutions  
of Polyethylene Oxide and Polyacrylamide
84. Ting, R.Y. & A.T. Ellis Phys Fluids 17 1461 (1974)  
Bubble Growth in Dilute Polymer Solutions
85. Truesdell, C. Springer-Verlag 1966  
The Elements of Continuum Mechanics

86. Truesdell, C. & W. Noll  
The non-Linear Field Theories of Mechanics  
in "Handbuch der Physik" Vol III/3  
ed by S. Flugge Springer-Verlag 1965
87. Tuck, E.O. JFM 18 619-635 (1964)  
Some Methods for Flows past Blunt Slender Bodies
88. Van Dyke, M. Academic Press 1964 229pp  
Perturbation Methods in Fluid Mechanics
89. Voinov, O.V. & V.V. Voinov  
Sov Phys Dokl 20 179-180 (1975)  
Numerical Method of Calculating Non-stationary Motions  
of an ideal incompressible fluid with free surfaces
90. ----- Sov Phys Dokl 21 133-135 (1976)  
On the Process of Collapse of a Cavitation Bubble near  
a Wall and the Formation of a Cumulative Jet
91. Wagner, M.G. & J.G. Slattery AIChEJ 17 1198-1207 (1971)  
Slow Flow of a non-Newtonian Fluid Past a Droplet
92. Whittaker, E.T. & G.N. Watson Cambridge 1965 608pp  
A Course of Modern Analysis
93. Zwick, S.A. & M.S. Plesset  
J Math & Phys 33 308-330 (1955)  
On the Dynamics of Small Vapor Bubbles in Liquids

APPENDIX

77-79

DISTRIBUTION LIST FOR UNCLASSIFIED  
TECHNICAL REPORTS AND REPRINTS ISSUED UNDER  
CONTRACT NR-74-038 TASK 162 637

All addressees receive one copy unless otherwise specified.

Defense Technical Information Center  
Cameron Station  
Alexandria, VA 22314 12 copies

Professor Bruce Johnson  
U.S. Naval Academy  
Engineering Department  
Annapolis, MD 21402

Library  
U.S. Naval Academy  
Annapolis, MD 21402

Technical Library  
David W. Taylor Naval Ship Research  
and Development Center  
Annapolis Laboratory  
Annapolis, MD 21402

Professor C. -S. Yih  
The University of Michigan  
Department of Engineering Mechanics  
Ann Arbor, MI 48109

Professor T. Francis Ogilvie  
The University of Michigan  
Department of Naval Architecture  
and Marine Engineering  
Ann Arbor, MI 48109

Office of Naval Research  
Code 211  
800 N. Quincy Street  
Arlington, VA 22217

Office of Naval Research  
Code 438  
800 N. Quincy Street  
Arlington, VA 22217 3 copies

Office of Naval Research  
Code 473  
800 N. Quincy Street  
Arlington, VA 22217

NASA Scientific and Technical  
Information Facility  
P. O. Box 8757  
Baltimore/Washington International  
Airport  
Maryland 21240

Professor Paul M. Naghdi  
University of California  
Department of Mechanical Engineering  
Berkeley, CA 94720

Librarian  
University of California  
Department of Naval Architecture  
Berkeley, CA 94720

Professor John V. Wehausen  
University of California  
Department of Naval Architecture  
Berkeley, CA 94720

Library  
David W. Taylor Naval Ship Research  
and Development Center  
Code 522.1  
Bethesda, MD 20084

Mr. Justin H. McCarthy, Jr.  
David W. Taylor Naval Ship Research  
and Development Center  
Code 1552  
Bethesda, MD 20084

Dr. William B. Morgan  
David W. Taylor Naval Ship Research  
and Development Center  
Code 1540  
Bethesda, MD 20084

Director, Office of Naval Research Eastern/  
Central Regional Office (Boston)  
Building 114, Section D  
666 Summer Street  
Boston, MA 02210

Library  
Naval Weapons Center  
China Lake, CA 93555

Technical Library  
Naval Surface Weapons Center  
Dahlgren Laboratory  
Dahlgren, VA 22418

Technical Documents Center  
Army Mobility Equipment Research Center  
Building 315  
Fort Belvoir, VA 22060

Technical Library  
Webb Institute of Naval Architecture  
Glen Cove, NY 11542

Dr. J. P. Breslin  
Stevens Institute of Technology  
Davidson Laboratory  
Castle Point Station  
Hoboken, NJ 07030

Professor Louis Landweber  
The University of Iowa  
Institute of Hydraulic Research  
Iowa City, IA 52242

R. E. Gibson Library  
The Johns Hopkins University  
Applied Physics Laboratory  
Johns Hopkins Road  
Laurel, MD 20810

Lorenz G. Straub Library  
University of Minnesota  
St. Anthony Falls Hydraulic Laboratory  
Minneapolis, MN 55414

Library  
Naval Postgraduate School  
Monterey, CA 93940

Technical Library  
Naval Underwater Systems Center  
Newport, RI 02840

Engineering Societies Library  
345 East 47th Street  
New York, NY 10017

The Society of Naval Architects and  
Marine Engineers  
One World Trade Center, Suite 1369  
New York, NY 10048

Technical Library  
Naval Coastal System Laboratory  
Panama City, FL 32401

Professor Theodore Y. Wu  
California Institute of Technology  
Engineering Science Department  
Pasadena, CA 91125

Director, Office of Naval Research Western  
Regional Office (Pasadena)  
1030 E. Green Street  
Pasadena, CA 91101

Technical Library  
Naval Ship Engineering Center  
Philadelphia Division  
Philadelphia, PA 19112

Army Research Office  
P. O. Box 12211  
Research Triangle Park, NC 27709

Editor  
Applied Mechanics Review  
Southwest Research Institute  
8500 Culebra Road  
San Antonio, TX 78206

Technical Library  
Naval Ocean Systems Center  
San Diego, CA 92152

ONR Scientific Liaison Group  
American Embassy - Room A-407  
APO San Francisco 96503

Librarian  
Naval Surface Weapons Center  
White Oak Laboratory  
Silver Spring, MD 20910

Defense Research and Development Attache  
Australian Embassy  
1601 Massachusetts Avenue, NW  
Washington, DC 20036

Page 3

Librarian Station 5-2  
Coast Guard Headquarters  
NASSIF Building  
400 Seventh Street, SW  
Washington, DC 20591

Library of Congress  
Science and Technology Division  
Washington, DC 20540

Dr. A. L. Slafkosky  
Scientific Advisor  
Commandant of the Marine Corps  
Code AX  
Washington, DC 20380

Maritime Administration  
Office of Maritime Technology  
14th & E Streets, NW  
Washington, DC 20230

Maritime Administration  
Division of Naval Architecture  
14th & E Streets, NW  
Washington, DC 20230

Dr. G. Kulin  
National Bureau of Standards  
Mechanics Section  
Washington, DC 20234

Naval Research Laboratory  
Code 2627  
Washington, DC 20375     6 copies

Library  
Naval Sea Systems Command  
Code 09GS  
Washington, DC 20362

Mr. Thomas E. Peirce  
Naval Sea Systems Command  
Code 03512  
Washington, DC 20362

Mr. Robert J. Dixon  
Boeing Marine Systems  
P. O. Box 3707, MS 17-01  
Seattle, WA 98124

110-79

DISTRIBUTION LIST FOR UNCLASSIFIED  
TECHNICAL REPORTS AND REPRINTS ISSUED UNDER  
CONTRACT N00014-77-0-0385 TASK 962-037

Professor Frederick G. Harmitt  
The University of Michigan  
Department of Mechanical Engineering  
Ann Arbor, MI 48109

Dr. Theodore R. Goodman  
Stevens Institute of Technology  
Davidson Laboratory  
Castle Point Station  
Hoboken, NJ 07030

Professor Albert T. Ellis  
University of California, San Diego  
Department of Applied Mechanics  
and Engineering Sciences  
La Jolla, CA 92093

Mr. Philip Eisenberg  
President, Hydronautics, Incorporated  
7210 Pindell School Road  
Laurel, MD 20810

Professor Allan J. Acosta  
California Institute of Technology  
Department of Mechanical Engineering  
Pasadena, CA 91125

Professor K. M. Agrawal  
Virginia State College  
Department of Mathematics  
Petersburg, VA 23803

Dr. A. Thiruvengadam  
Daedalean Associates, Inc.  
Springlake Research Center  
15110 Frederick Road  
Woodbine, MD 21797